

From spin squeezing to fast state discrimination

Michael R. Geller^{1,2}

¹Department of Physics and Astronomy, University of Georgia, Athens, Georgia 30602, USA

²Center for Simulational Physics, University of Georgia, Athens, Georgia 30602, USA

October 28, 2024

There is great interest in generating and controlling entanglement in Bose-Einstein condensates and similar ensembles for use in quantum computation, simulation, and sensing. One class of entangled states useful for quantum-enhanced metrology are spin-squeezed states of N two-level atoms. After preparing a spin coherent state of width $N^{-\frac{1}{2}}$ centered at coordinates (θ, ϕ) on the Bloch sphere, atomic interactions generate a nonlinear evolution that shears the state's probability density, stretching it to an ellipse and causing squeezing in a direction perpendicular to the major axis. Here we consider the same setup but in the $N \rightarrow \infty$ limit (simultaneously rescaling scattering lengths by $1/N$). This shrinks the initial coherent state to zero area. Large N also suppresses two-particle entanglement and squeezing, as required by a monogamy bound. The torsion (1-axis twist) is still present, however, and the center (θ, ϕ) of the large N coherent state evolves as a qubit governed by a two-state Gross-Pitaevskii equation. The resulting nonlinearity is known to be a powerful resource in quantum computation. In particular, it can be used to implement single-input quantum state discrimination, an impossibility within linear one-particle quantum mechanics. In this problem, a qubit state $|\psi\rangle \in \{|a\rangle, |b\rangle\}$ is input to a procedure (with knowledge of the candidates $|a\rangle, |b\rangle$) that attempts to determine which was provided. We obtain a solution to the discrimination problem in terms of a Viviani curve on the Bloch sphere. We also consider an open-system variant containing both Bloch sphere torsion and dissipation. In this case it should be possible to generate two basins of attraction within the Bloch ball, having a shared boundary that can be used for a type of autonomous state discrimination that is independent of $|a\rangle, |b\rangle$. We explore these and other connections between spin squeezing in the large N limit and nonlinear quantum gates, and argue that a two-component condensate is a promising platform for realizing a nonlinear qubit.

arXiv:2410.22032v1 [quant-ph] 29 Oct 2024

Michael R. Geller: mgeller@uga.edu

Contents

1	Introduction	2
1.1	Squeezing and nonlinear gates	2
1.2	Reduction of 3SAT to state discrimination	3
1.3	Trading time complexity for space complexity	4
1.4	Coupling linear and nonlinear qubits	5
1.5	Large N limit and 2-particle entanglement	5
1.6	Summary of results	7
2	Bloch sphere torsion and squeezing	7
2.1	Trace distance monotonicity	7
2.2	Nonlinear qubit with torsion	8
2.3	Microscopic model	9
2.4	Path integral and large N limit	11
3	Single-input state discrimination	12
3.1	Torsion and conservation laws	12
3.2	State discrimination along Viviani's curve	13
3.3	Kitagawa-Ueda model as $N \rightarrow \infty$	14
4	Fast discrimination with torsion and dissipation	15
4.1	Combining contractive and expansive dynamics	15
4.2	Jump operators	16
4.3	Fixed points	18
4.4	Autonomous state discrimination	19
5	Discussion	19
A	Entanglement monogamy	20
B	Monotonicity of trace distance	22

1 Introduction

1.1 Squeezing and nonlinear gates

A major theme in quantum sensing and metrology is the use of entanglement to improve the precision of parameter estimation beyond the standard quantum limit [1–17]. It has long been recognized that atomic Bose-Einstein condensates (BEC) and quantum spin ensembles provide natural platforms for preparing and controlling the squeezed states sufficient for achieving this sensitivity enhancement [4–17]. In the case of a two-component condensate with tunable atomic interaction, the SU(2) coherent state [18–21]

$$|F\rangle := \frac{(\psi_0 a_0^\dagger + \psi_1 a_1^\dagger)^N}{\sqrt{N!}} |\text{vac}\rangle, \quad \psi_{0,1} \in \mathbb{C}, \quad \psi_0 = \cos\left(\frac{\theta}{2}\right), \quad \psi_1 = e^{i\phi} \sin\left(\frac{\theta}{2}\right), \quad (1)$$

is prepared, centered at coordinates (θ, ϕ) on the Bloch sphere. Here $\psi_0 a_0^\dagger + \psi_1 a_1^\dagger$ creates an atom in a superposition of spin or internal components 0 and 1, and N is the number of qubits (two-level atoms). The $a_{0,1}$ are bosonic annihilation operators for the two internal states. The initial state (1) is separable and is simplest to prepare with the interaction turned off.

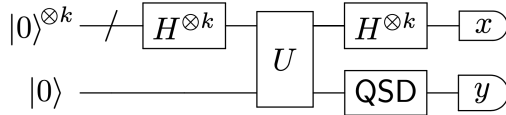


Figure 1: Efficient reduction of 3SAT to quantum state discrimination (QSD). Here U implements the oracle and the first register is postselected to $|0\rangle^{\otimes k}$. The QSD gate implements fast discrimination by simulating a nonlinear qubit. The output of QSD is always a classical state $|0\rangle$ or $|1\rangle$.

The many-body state (1), parameterized by coordinates (θ, ϕ) , encodes a single qubit: The same probability amplitudes $\psi_{0,1}$ are stored in each of N identical bosons. Atomic interactions then generate a nonlinear Hamiltonian, such as the Kitagawa-Ueda one-axis-twist spin model [4], which shears the state’s probability density, stretching it to an ellipse and squeezing the state in a direction perpendicular to the major axis [4–17].

In this paper we argue that the Bloch sphere torsion responsible for enhanced metrology through squeezing can also be used to enhance quantum computation. It is known that nonlinear quantum evolution in idealized models can significantly enhance information processing [22–40]. This is true even if there is only *one* nonlinear qubit coprocessor coupled to a linear and otherwise conventional quantum computer [22, 23, 40]. In this simplified setting, there is already an efficient reduction from any problem in the complexity class NP—for which it is possible to efficiently check a proposed solution—to the problem of discriminating exponentially close single-qubit states $|a\rangle$ and $|b\rangle$ [22, 23]. By *efficient reduction* we mean a polynomial-depth quantum circuit for solving one problem in terms of another. Discriminating $|a\rangle$ and $|b\rangle$ means inputting $|\psi\rangle \in \{|a\rangle, |b\rangle\}$ into a procedure that determines whether $|\psi\rangle$ is $|a\rangle$ or $|b\rangle$; normally this requires many perfect copies of the input [41–44].

1.2 Reduction of 3SAT to state discrimination

To understand the reduction, note that it is sufficient to reduce the Boolean satisfiability problem 3SAT to state discrimination, because 3SAT is NP-complete [45]. Each instance is specified by a Boolean function $f : \mathbb{Z}_2^k \rightarrow \mathbb{Z}_2$ on k bits, in conjunctive normal form (product of clauses) with clauses containing no more than three input bits or their negations. The 3SAT problem asks if there is at least one assignment $x \in \mathbb{Z}_2^k$ such that $f(x) = 1$ (TRUE). If f is always 0 (FALSE) then f is unsatisfiable. The reduction given by Abrams and Lloyd [22] assumes an efficient gate decomposition for the *oracle* operator $U|x\rangle|y\rangle = |x\rangle|y \oplus f(x)\rangle$, as well as access to a fault-tolerant quantum computer. Here \oplus denotes addition mod 2.

The reduction circuit, shown in Figure 1, measures a global property of f (number of satisfying assignments) by one application of the oracle to a uniform superposition of classical states $\{|x\rangle\}_{x \in \mathbb{Z}_2^k}$. Initialize k qubits and an ancilla qubit to $|0\rangle^{\otimes k}|0\rangle$. Next apply Hadamard gates $H^{\otimes k}$ to the first k qubits, where $H^{\otimes k}|x\rangle = 2^{-\frac{k}{2}} \sum_{x' \in \mathbb{Z}_2^k} (-1)^{\sum_i x_i x'_i} |x'\rangle$. This leads to $2^{-\frac{k}{2}} \sum_{x \in \mathbb{Z}_2^k} |x\rangle|0\rangle$. Applying the oracle U leads to

$$\frac{1}{\sqrt{2^k}} \sum_{x \in \mathbb{Z}_2^k} |x\rangle |f(x)\rangle. \quad (2)$$

A second application of $H^{\otimes k}$ then leads to

$$\frac{1}{2^k} \sum_{x \in \mathbb{Z}_2^k} \sum_{x' \in \mathbb{Z}_2^k} (-1)^{\sum_i x_i x'_i} |x'\rangle |f(x)\rangle \quad (3)$$

$$= |0\rangle^{\otimes k} \frac{(2^k - s)|0\rangle + s|1\rangle}{2^k} + \frac{1}{2^k} \sum_{x \in \mathbb{Z}_2^k} \sum_{x' \neq 0^k} (-1)^{\sum_i x_i x'_i} |x'\rangle |f(x)\rangle, \quad (4)$$

where s is the number of satisfying assignments. Measuring the first k qubits results in a classical output we call $x \in \mathbb{Z}_2^k$, as indicated by the final measurement gate in Figure 1. Postselecting for $x = 0$ gives $|0\rangle^{\otimes k} |\text{out}(s)\rangle$ with probability $\frac{(2^k - s)^2 + s^2}{2^{2k}} \geq \frac{1}{2}$, where

$$|\text{out}(s)\rangle := \frac{(2^k - s)|0\rangle + s|1\rangle}{\sqrt{(2^k - s)^2 + s^2}}, \quad 1 \leq s \leq 2^k. \quad (5)$$

Distinguishing the cases $s = 0$ (f is not satisfiable) and $s > 0$ (f is satisfiable) is therefore equivalent to discriminating the ancilla states [22, 23]

$$|a\rangle = |\text{out}(s=0)\rangle \quad \text{and} \quad |b\rangle = |\text{out}(s>0)\rangle. \quad (6)$$

This reduction is not useful for linear quantum computers, however, because in the hard case where there are only a few $s \ll 2^k$ satisfying assignments, the states $|a\rangle$ and $|b\rangle$ are very similar. Their overlap $\langle a|b\rangle = 1 - \frac{s^2}{2} 2^{-2k} + O(2^{-3k})$, $|\langle a|b\rangle|^2 = 1 - s^2 2^{-2k} + O(2^{-3k})$, when $k \gg 1$ and $s \ll 2^k$, is exponentially close to unity. It is well known that discrimination protocols based on linear gates require exponential resources in this case [41–44], reflecting the limited information gained through measurement. So the reduction based on Figure 1 does not allow one to solve NP-complete problems efficiently with a linear computer.

Abrams and Lloyd [22] explored the implications of hypothetical forms of Schrödinger equation nonlinearity (which have not been observed experimentally [46–56]) on the power of quantum computers, and argued that even simple types would enable *single-input* quantum state discrimination (QSD) of exponentially close states, enabling polynomial-time solution of NP-complete problems (and beyond). It should be emphasized that linear quantum computers are not expected to solve NP-complete problems efficiently (factoring is in NP but is not NP-complete) [57]. So it's interesting to investigate the power of nonlinearity further [22–40]. An interesting series of papers assumed the Gross-Pitaevskii nonlinearity [58, 59] used to model ground states of dilute weakly interacting bosons in a mean-field approximation, finding speedups for both searching [23, 32–35] and QSD [23]. But specific experimental proposals for their implementation have not been available until recently [39, 40], and none of the protocols have been demonstrated.

The objective of this paper is to argue that the nonlinearity responsible for spin squeezing can also be harnessed for fast QSD. This is the subject of Sections 2 and 3. In Section 4 we discuss a variation obtained by combining Bloch sphere torsion with dissipation, leading to a pair of basins of attraction within the Bloch ball that can be used to implement a form of *autonomous* QSD. The nonlinear approach is summarized and its limitations are discussed in Section 5.

We conclude this section with some comments on complexity (Section 1.3), coupling to and entangling with linear qubits (Section 1.4), and the large N limit and entanglement monogamy (Section 1.5). The main results are also summarized (Section 1.6).

1.3 Trading time complexity for space complexity

The first comment regards speedup: Every BEC is an N -body system governed by linear quantum mechanics, so how can it provide nonlinear speedup? In the nonlinear approach,

that same BEC is (approximately) described by a one-body problem with self-interaction, and the accuracy of the nonlinear picture requires N to be large. The atomic gas is used as a register of bosonic qubits initialized into a symmetric product state (1) via condensation, and subsequently controlled by varying the interaction. Time speedup is possible here because we have traded time complexity for space complexity: In the nonlinear picture there is only one qubit. The exponential time cost for discriminating exponentially close states with a linear quantum computer is transformed to a large N requirement.

How large? The answer depends on the desired accuracy of the mean field theory. In a large family of condensate models (with $1/N$ scaling of the interaction) it is possible to rigorously upper bound the *model error* $\epsilon := \|\rho_{\text{eff}}(t) - \rho_1(t)\|_1$ by

$$\epsilon \leq c \frac{e^{t/t_{\text{ent}}} - 1}{N}, \quad (7)$$

where t is the evolution time (assuming the condensate is initialized to a symmetric product state at $t=0$), and where c and t_{ent} are positive constants (model-dependent parameters independent of t and N) [60, 61]. Here ρ_{eff} is the mean field state, ρ_1 is the exact state traced over all qubits but one, and $\|\cdot\|_1$ is the trace norm (Schatten 1-norm)

$$\|X\|_1 := \text{tr}(|X|), \quad |X| = \sqrt{X^\dagger X}. \quad (8)$$

The exponential growth of the worst case error in (7) is to be expected, with a rate determined by the type, strength, and range of the interaction [62]. The $1/N$ dependence reflects two-particle entanglement monogamy (discussed below). We see from (7) that there is a short-time window $t < t_{\text{ent}}$ where the required number of condensed atoms $N \approx c/\epsilon$ is constant (for fixed ϵ). This is because the BEC is initialized into a product state, and it takes a time t_{ent} for the atomic collisions to produce entanglement. However for long computations, exponentially many atoms $N \approx (c/\epsilon)e^{t/t_{\text{ent}}}$ are required. Long computations would also require error correction, which is not addressed here.

1.4 Coupling linear and nonlinear qubits

The second comment concerns entanglement between a scalable quantum computer and the nonlinear coprocessor. To solve a given 3SAT instance, the linear qubits are entangled with the nonlinear qubit (encoded in a BEC) in step (2). This requires coupling a conventional qubit to a condensate in a controllable fashion.

One promising approach builds on advances combining cold atom magneto-optical traps or optical lattices with electromagnetic traps for ions [63–72]. Theoretical proposals have been explored for entangling trapped-ion qubits with BECs and verifying ion-condensate entanglement (ICE) [70–72]. A recent proposal by Großardt [40] considers a neutral atom qubit coupled to a BEC. Ions immersed in a BEC have demonstrated sympathetic cooling of the ions [68, 69], but ICE has not been demonstrated experimentally.

1.5 Large N limit and 2-particle entanglement

The final comment concerns the large N limit. The standard model for a scalar condensate [73–76] on which the Gross-Pitaevskii equation is based is that of a dilute Bose gas at zero temperature with the short-range atomic interaction replaced by a contact interaction:

$$V_{\text{int}}(\mathbf{r} - \mathbf{r}') \approx U_0 \delta(\mathbf{r} - \mathbf{r}'), \quad U_0 = \frac{4\pi\hbar^2 a_s}{m}, \quad (9)$$

where a_s is the s-wave scattering length and m is the atomic mass. The use of the contact interaction requires low energy and dilute neutral atoms such that $r_{\text{ave}} \gg |a_s|$, where r_{ave}

is the average inter-particle distance. In addition, the Gross-Pitaevskii equation is a mean field approximation, so $N \gg 1$ is also required to suppress fluctuations. Thus, as is well known, the use of the Gross-Pitaevskii equation to model a BEC requires both $r_{\text{ave}} \gg |a_s|$ and $N \gg 1$, as well as low energy and temperature [74]. However the Gross-Pitaevskii equation can become invalid in the $N \rightarrow \infty$ limit (even while remaining dilute). This limit is especially problematic in multi-component BECs, where only the lowest energy (spatial or internal) modes are included in a model, the others neglected on account of their higher energy. But with a_s fixed, the ground state energy per particle can diverge as $N \rightarrow \infty$, invalidating the low energy assumptions. To avoid this, we adopt the approach of rigorous investigations of the Gross-Pitaevskii equation by simultaneously rescaling scattering lengths by $1/N$ as $N \rightarrow \infty$ [77–90], making the large N limit well defined. In particular, the error bound (7) assumes this rescaling of the interaction. Thus, the nonlinear picture is best understood theoretically in the double limit $N \rightarrow \infty$, $a_s \rightarrow 0$, with Na_s held constant.

The $1/N$ dependence in (7) is anticipated from a monogamy inequality [91, 92] for pairwise entanglement when applied to a system with permutation symmetry. To see this, first note that $\|\rho_{\text{eff}}(t) - \rho_1(t)\|_1 = |\vec{r}_{\text{eff}} - \vec{r}_1|$ measures both unitary and nonunitary errors in the mean field state ρ_{eff} , by which we mean differences in the Bloch vector orientation and length. However due to the symmetry of the interaction (9) the error here is mainly nonunitary, caused by the pairwise (and higher order) entanglement of qubit 1 with 2, 3, \dots , N and its resulting entropy increase. So we can assume that the model error ϵ is predominantly a nonunitary error caused by pairwise entanglement. Let $\tau(\rho_{ij})$ be the *tangle* (concurrence squared) between qubits i and j , a measure of their shared entanglement detected via the two-qubit density matrix ρ_{ij} , traced over other atoms. The tangle satisfies the monogamy inequality [91, 92]

$$\tau(\rho_{12}) + \tau(\rho_{13}) + \dots + \tau(\rho_{1N}) \leq 4 \det(\rho_1), \quad N \geq 3. \quad (10)$$

The left side is a sum of the tangles (each quantifying two-qubit entanglement) between qubits 1 and 2, between 1 and 3, and so on. The right side is a measure of the total entanglement of qubit 1 with the ensemble, including genuine multiparticle entanglement, detected via the reduced density matrix ρ_1 (note that every qubit state ρ has $\det \rho \leq \frac{1}{4}$). If the system has permutation symmetry, the tangles are equal and satisfy an intuitive bound

$$\tau(\rho_{ij}) \leq \frac{1}{N-1}. \quad (11)$$

This has the same large N behavior as the model error bound (7). As previously noted by Yang [93], the pairwise entanglement (as measured by concurrence or tangle) in any permutation-symmetric state always vanishes in the large N limit:

$$\lim_{N \rightarrow \infty} \tau(\rho_{ij}) = 0. \quad (12)$$

In the nonlinear approach to information processing, entanglement is intentionally suppressed this way. Although the proof of inequality (10) for general N is somewhat complicated and took several years to complete [92, 93] after the initial proof for $N = 3$ [91], a simpler derivation is possible here due to the assumed permutation symmetry; this is provided in Appendix A. For explicit calculations of concurrence in a variety of symmetric multiqubit states, including squeezed states, see Wang and Mølmer [94] and Wang and Sanders [7].

1.6 Summary of results

This paper is mainly a proposal for experiments at the interface of atomic physics, nonlinear quantum mechanics, and quantum information. The goal of the paper is to explain why they would be interesting, and to offer conventional (if somewhat idealized) microscopic models for their description. The connections explored here between spin squeezing, expansive dynamics, and nonlinear gates is likely to be applicable beyond the specific physical platform and squeezing mechanism considered here. The main contributions are:

- (i) We propose to use an ultracold gas of N neutral two-level atoms to implement an encoded qubit evolving nonlinearly in time according to the Gross-Pitaevskii equation, with the accuracy controlled by N . Atom-atom entanglement is intentionally suppressed by making N large, using bound (11), and interactions weak. Speedup of state discrimination is possible because the exponential time cost is replaced by an exponential space cost. To enhance the power of a scalable quantum computer, the nonlinear coprocessor is entangled with a register of conventional qubits.
- (ii) We obtain conservation laws satisfied by the torsion model, and use them to design a single-input state discrimination gate based on Viviani's curve (Section 3). After the gate, input $|a\rangle$ is mapped to $|0\rangle$, and $|b\rangle$ is mapped to $|1\rangle$.
- (iii) We consider a dissipative torsion model containing a phase where the Bloch ball develops two basins of attraction \mathbb{V}_+ and \mathbb{V}_- flowing to opposing fixed points $\mathbf{r}_+^{\text{fp}}, \mathbf{r}_-^{\text{fp}}$. We propose to use this dynamical system to implement an autonomous quantum state discrimination gate that maps every input state in \mathbb{V}_+ to \mathbf{r}_+^{fp} , and every state in \mathbb{V}_- to \mathbf{r}_-^{fp} (Section 4).

2 Bloch sphere torsion and squeezing

2.1 Trace distance monotonicity

To understand the importance of torsion and related concepts in nonlinear qubit models, it is useful to clarify precisely how nonlinear evolution might benefit information processing. After all, single-qubit operations such as state preparation, unitary gates, and readout are routinely demonstrated with very high precision. Nonlinearity appears to offer no benefit for these operations [95]. Instead, consider how the entire state space—the Bloch ball—flows under some continuous evolution, such as that generated by the Gorini-Kossakowski-Sudarshan-Lindblad master equation [96, 97]. This geometric perspective focuses on the trajectories of a given state together with those nearby. Unitary gates rotate the Bloch ball rigidly around a fixed axis. We can say that unitary evolution on a pair of states (ρ_a, ρ_b) is distance-preserving, where the distance $\|\rho_a - \rho_b\|_1$ is measured in trace norm. (For qubits with Bloch vectors $\vec{r}_{a,b}$, we note that $\|\rho_a - \rho_b\|_1 = \text{tr}|\frac{\vec{r}_a - \vec{r}_b \cdot \vec{\sigma}}{2}| = |\vec{r}_a - \vec{r}_b|$.) Dissipation and decoherence eventually map all states to a ground or mixed state. So nonunitary evolution is always contractive: quantum states (in the space of density matrices) move closer over time. But time evolution never moves a pair of states apart or decreases their overlap.

This restriction is captured by the *monotonicity* of trace distance [98] (or relative entropy [99]) under linear time evolution: Let $\rho_a, \rho_b \in \mathbb{C}^{d \times d}$ be states (positive semidefinite operators with unit trace), and let ϕ be a *linear* positive trace-preserving channel (complete positivity is not required). Then

$$\|\phi(\rho_a) - \phi(\rho_b)\|_1 \leq \|\rho_a - \rho_b\|_1. \quad (13)$$

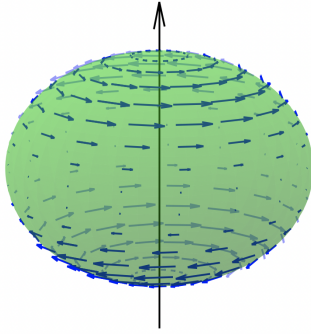


Figure 2: Block ball subjected to z -axis torsion. All states in the upper hemisphere are expansive with all states in the lower hemisphere, a powerful quantum information processing resource.

The trace norm is physically relevant because the normalized trace distance

$$D(\rho_a, \rho_b) := \frac{\|\rho_a - \rho_b\|_1}{2} = \max_{0 \preceq E \preceq I} \text{tr}[(\rho_a - \rho_b)E], \quad 0 \leq D(\rho_a, \rho_b) \leq 1, \quad (14)$$

quantifies the distinguishability of (ρ_a, ρ_b) by any single (projective or POVM) measurement operator $E \in \mathbb{C}^{d \times d}$ [98]. The standard reference for (13) is Ruskai [99], who proved a more general monotonicity condition that includes (13) as a special case (but assumes complete positivity). Additional discussion of trace distance monotonicity and a direct proof of (13) are provided in Appendix B.

2.2 Nonlinear qubit with torsion

A variety of nonlinear evolution equations, however, are known to violate trace distance monotonicity [22, 23, 38], enabling a potential computational advantage that we explore here. A popular model for single-qubit nonlinearity is the z -axis torsion model [23, 38] proposed by Mielnik [95] in 1980:

$$\frac{d\rho}{dt} = -i[H_{\text{eff}}, \rho], \quad H_{\text{eff}} = g \text{tr}(\rho\sigma^z)\sigma^z, \quad \rho, H_{\text{eff}} \in \mathbb{C}^{2 \times 2}. \quad (15)$$

This Hamiltonian generates z rotation with a frequency $2g \text{tr}(\rho\sigma^z)$ proportional to the z coordinate of the state, as illustrated in Figure 2. Under this evolution an initial Bloch vector $\vec{r} = \text{tr}(\rho\vec{\sigma})$ is subjected to a state-dependent rotation, a feature absent in the $\text{SU}(2)$ gate set. For example, states in the upper hemisphere in Figure 2 rotate in the opposite direction to those in the lower hemisphere. Pairs of such states move apart from each other and violate trace distance monotonicity. Torsion about x and y are similarly generated by $\text{tr}(\rho\sigma^x)\sigma^x$ and $\text{tr}(\rho\sigma^y)\sigma^y$.

The expansivity can be used to implement single-input QSD [22, 23, 38], an impossibility in linear one-particle quantum mechanics [41–44]. We will assume that $g \in \mathbb{R}$ is experimentally controllable and that linear Hermitian operators can be added to H_{eff} to implement arbitrary $\text{SU}(2)$ gates. The torsion model (15) is not microscopic, but effective, arising from a family of distinct microscopic models in their large N limits.

In a recent paper [39], we mapped an atomtronic SQUID [100–106] to the torsion model and used it to design a single-input QSD gate for a nonlinear qubit encoded in a rotating toroidal condensate. In this work we map a trapped two-component atomic BEC to the torsion model, and design fast discriminators for this setup as well. A potential

advantage of the two-component realization is that spin squeezing is now highly advanced and demonstrated by many labs worldwide [4–17]. Another is pedagogical: In the two-component BEC, the case of pure torsion can be calculated exactly from the Kitagawa-Ueda spin model [4] in the large spin limit, confirming the mean field prediction.

2.3 Microscopic model

In this section, we briefly review a two-component BEC model and use it to recover known spin squeezing results. Then in Sec. 2.4 we take the large N limit and obtain the torsion model (15). We consider a dilute condensate of trapped bosonic atoms of mass m and metastable internal states $|\Psi_0\rangle$, $|\Psi_1\rangle$ at zero temperature [19]:

$$H = \sum_{\alpha=0,1} \int d^3r \left(\phi_\alpha^\dagger T_\alpha \phi_\alpha + \frac{U_{\alpha\alpha}}{2} \phi_\alpha^\dagger \phi_\alpha^\dagger \phi_\alpha \phi_\alpha \right) + U_{01} \int d^3r \phi_0^\dagger \phi_1^\dagger \phi_0 \phi_1 + \frac{\Omega}{2} \int d^3r (\phi_0^\dagger \phi_1 + \phi_1^\dagger \phi_0), \quad (16)$$

where $T_\alpha = -\frac{\nabla^2}{2m} + V_{\text{ext},\alpha}(\mathbf{r})$ is a single-atom Hamiltonian with state-dependent trapping potential $V_{\text{ext},\alpha}(\mathbf{r}) = \frac{1}{2}m\omega_\alpha^2 r^2$. Here $[\phi_\alpha(\mathbf{r}), \phi_{\alpha'}^\dagger(\mathbf{r}')] = \delta_{\alpha\alpha'} \delta(\mathbf{r} - \mathbf{r}')$, where $\phi_\alpha^\dagger(\mathbf{r})$ acting on the vacuum creates an atom centered at position \mathbf{r} in state $|\Psi_\alpha\rangle$. We also assume that $\langle \Psi_0 | \Psi_1 \rangle = 0$. Interaction parameters U_{00} , U_{01} , and U_{11} have the form of (9) with three scattering lengths characterizing the three independent types of binary collisions. The last term in (16) describes resonant laser-driven transitions between $|\Psi_0\rangle$ and $|\Psi_1\rangle$ with frequency Ω .

Atoms are condensed into Gaussian translational modes $f_0(\mathbf{r})$ and $f_1(\mathbf{r})$:

$$\phi_\alpha(\mathbf{r}) = f_\alpha(\mathbf{r}) a_\alpha, \quad f_\alpha(\mathbf{r}) = \frac{e^{-r^2/2\ell_\alpha^2}}{(\pi\ell_\alpha^2)^{3/4}}, \quad \ell_\alpha = \sqrt{\frac{\hbar}{m\omega_\alpha}}, \quad \alpha \in \{0, 1\}, \quad (17)$$

where $\int d^3r f_\alpha f_\beta = [\frac{2\ell_\alpha\ell_\beta}{\ell_\alpha^2 + \ell_\beta^2}]^{3/2}$ and $\int d^3r f_\alpha^2 f_\beta^2 = [\frac{1}{\pi(\ell_\alpha^2 + \ell_\beta^2)}]^{3/2}$ (spatial modes are not orthogonal). Here a_α^\dagger creates an atom with internal state α in a harmonic oscillator ground state $f_\alpha(\mathbf{r})$ satisfying $T_\alpha f_\alpha(\mathbf{r}) = \frac{\omega_\alpha}{2} f_\alpha(\mathbf{r})$, and $[a_\alpha, a_\beta^\dagger] = \delta_{\alpha\beta}$. Then

$$H = \sum_{\alpha=0,1} \left(\frac{\omega_\alpha}{2} a_\alpha^\dagger a_\alpha + \gamma_\alpha a_\alpha^\dagger a_\alpha^\dagger a_\alpha a_\alpha \right) + \gamma' a_0^\dagger a_1^\dagger a_0 a_1 + \lambda (a_0^\dagger a_1 + a_1^\dagger a_0), \quad (18)$$

where

$$\gamma_\alpha = \frac{U_{\alpha\alpha}}{2(2\pi\ell_\alpha^2)^{3/2}}, \quad \gamma' = \frac{U_{01}}{[\pi(\ell_0^2 + \ell_1^2)]^{3/2}}, \quad \lambda = \frac{\Omega}{2} \left(\frac{2\ell_0\ell_1}{\ell_0^2 + \ell_1^2} \right)^{3/2}. \quad (19)$$

We will use the two-mode model (18) as the basis of our investigations. In the remainder of this section, we transform to the angular momentum representation and analyze squeezing. The spin- $\frac{N}{2}$ Schwinger boson representation of $\text{SU}(2)$ generators is given by

$$J_x = \frac{a_0^\dagger a_1 + a_1^\dagger a_0}{2}, \quad J_y = i \frac{a_1^\dagger a_0 - a_0^\dagger a_1}{2}, \quad J_z = \frac{a_0^\dagger a_0 - a_1^\dagger a_1}{2}, \quad N = a_0^\dagger a_0 + a_1^\dagger a_1. \quad (20)$$

These satisfy

$$J_+ = J_x + iJ_y = a_0^\dagger a_1, \quad J_- = J_x - iJ_y = a_1^\dagger a_0 = J_+^\dagger, \quad (21)$$

$$[J^\mu, J^\nu] = i\epsilon^{\mu\nu\lambda} J^\lambda, \quad [J_z, J_\pm] = \pm J_\pm, \quad [J_+, J_-] = 2J_z. \quad (22)$$

To analyze squeezing it is sufficient to consider $\Omega = 0$ and $N \gg 1$. In this case (18) becomes

$$H = \left(\frac{\omega_0 + \omega_1}{4}\right)N + \left(\frac{\gamma_0 + \gamma_1 + \gamma'}{4}\right)N^2 + \left(\frac{\omega_0 - \omega_1}{2}\right)J_z + (\gamma_0 - \gamma_1)NJ_z + \chi J_z^2, \quad (23)$$

where

$$\chi := \gamma_0 + \gamma_1 - \gamma'. \quad (24)$$

Setting $\omega_0 = \omega_1$, $\gamma_0 = \gamma_1$, and dropping additive constants leads to the Kitagawa-Ueda one-axis twist model:

$$H_{\text{KU}} = \chi J_z^2. \quad (25)$$

First prepare a coherent state (1) centered at the $|+\rangle$ state on the Bloch sphere:

$$|F_+\rangle = \frac{(a_0^\dagger + a_1^\dagger)^N}{\sqrt{2^N} \sqrt{N!}} |\text{vac}\rangle. \quad (26)$$

The angular momentum in the initial state (26) is

$$\langle J_x \rangle = \frac{N}{2}, \quad \langle J_y \rangle = \langle J_z \rangle = 0, \quad \langle J_x^2 \rangle = \frac{N^2}{4}, \quad \langle J_y^2 \rangle = \langle J_z^2 \rangle = \frac{N}{4}, \quad (27)$$

and the variances are $\text{Var}(J_x) = 0$ and $\text{Var}(J_y) = \text{Var}(J_z) = \frac{N}{4}$. We note that $|F_+\rangle$ is a minimum-uncertainty state satisfying

$$\text{Var}(J_y) = \text{Var}(J_z) = \frac{|[\langle J_y, J_z \rangle]|}{2} = \frac{\langle J_x \rangle}{2} = \frac{N}{4}. \quad (28)$$

Next turn on the atomic interaction (with $\omega_0 = \omega_1$ and $\gamma_0 = \gamma_1$). This leads, in the spin picture, to the Kitagawa-Ueda Hamiltonian (25). After evolution for a time t the state becomes $U|F_+\rangle$, where $U = e^{-i\chi t J_z^2}$. The squeezing occurs in the yz plane, so define

$$J_\varphi := \sin(\varphi)J_y + \cos(\varphi)J_z, \quad (29)$$

and calculate the expectation and variance of J_φ as a function of angle φ . Use the identity

$$U^\dagger J_+ U = J_+ e^{2i\chi t J_z} e^{i\chi t}, \quad U = e^{-i\chi t J_z^2}, \quad (30)$$

to obtain

$$\langle J_\varphi \rangle = \langle F_+ | U^\dagger J_\varphi U | F_+ \rangle = 0, \quad t \geq 0, \quad (31)$$

and [94]

$$\text{Var}(J_\varphi) = \frac{N}{4} + \frac{N^2}{8} \left[1 - \cos^{N-2}(2\chi t) \right] \sin^2(\varphi) + \frac{N^2}{4} \cos^{N-2}(\chi t) \sin(\chi t) \sin(2\varphi), \quad (32)$$

where we have used $N \gg 1$. The two-mode model (18) correctly recovers established properties of spin squeezed condensates [4–17].

2.4 Path integral and large N limit

Next we take the $N \rightarrow \infty$ limit and explain how to perform single-input QSD with the same Hamiltonian (18). This is an adaptation of [39] to the two-component BEC. To use the BEC as a nonlinear qubit, we need to control the accuracy of mean field theory by making N large and leveraging entanglement monogamy. This keeps the many-body wave function close to a coherent state (1) for some qubit coordinates (probability amplitudes) $\psi_{0,1} \in \mathbb{C}$, even when the interaction is turned on (without loss of generality we assume here that ψ_0 is real and nonnegative). The only relevant dynamical variables in this limit are the coordinates themselves, and we are interested in their propagator $\langle F|e^{-iHt}|F'\rangle$. Here $|F\rangle$ and $|F'\rangle$ are states of the form (1), with qubit coordinates $\psi_{0,1}$ and $\psi'_{0,1}$ respectively.

In some cases it is possible to calculate the dynamics exactly for any N (Section 3.3). More generally we seek a simplified description of the problem, made possible by large N . Note that $\langle F|F'\rangle = \langle \psi|\psi'\rangle^N$, where $\langle \psi|\psi'\rangle = \bar{\psi}_0\psi'_0 + \bar{\psi}_1\psi'_1$ is the single-atom overlap (and $|\langle \psi|\psi'\rangle| \leq 1$). Here \bar{z} denotes complex conjugation. It follows that, for any $|F\rangle \neq |F'\rangle$, we must have $\lim_{N \rightarrow \infty} \langle F|F'\rangle = 0$. This orthogonality catastrophe defines a quasiclassical limit for the model (distinct from the $\hbar \rightarrow 0$ limit). The coherent states occupy a subspace of two-mode Fock space that we call \mathcal{H}_{coh} . Let $|n_0, n_1\rangle := \frac{(a_0^\dagger)^{n_0}}{\sqrt{n_0!}} \frac{(a_1^\dagger)^{n_1}}{\sqrt{n_1!}} |\text{vac}\rangle$.

Expanding (1) in this basis leads to $|F\rangle = \sum_{k=0}^N \sqrt{\binom{N}{k}} \psi_0^{N-k} \psi_1^k |N-k, k\rangle$, where $\binom{N}{k}$ is the binomial coefficient. Therefore $\dim(\mathcal{H}_{\text{coh}}) = N+1$. Averaging the pure state $|F\rangle\langle F|$ over the Bloch sphere yields a maximally mixed state $\int \frac{\sin(\theta)d\theta d\phi}{4\pi} |F\rangle\langle F| = \frac{I_{N+1}}{N+1}$, where $I_{N+1} = \sum_{k=0}^N |N-k, k\rangle\langle N-k, k|$ is the identity in \mathcal{H}_{coh} . Now split the evolution into $K \gg 1$ short-time propagators. This leads to $\langle F|e^{-iHt}|F'\rangle = \langle F|(e^{-iH\tau})^K|F'\rangle = \int (\prod_{k=1}^{K-1} \frac{N+1}{4\pi} \sin \theta_k d\theta_k d\phi_k) \prod_{k=1}^K \langle F_k|e^{-iH\tau}|F_{k-1}\rangle$, where $|F_0\rangle = |F'\rangle$, $|F_K\rangle = |F\rangle$, and $\tau = t/K$. For small τ and large N we have

$$\begin{aligned} \langle F|e^{-iH\tau}|F'\rangle &= \langle F|F'\rangle \left\{ 1 - iN\tau \left[\sum_{\alpha} \left(\frac{\omega_{\alpha}}{2} \bar{\psi}_{\alpha}\psi_{\alpha} + \gamma_{\alpha}N \bar{\psi}_{\alpha}\bar{\psi}_{\alpha}\psi_{\alpha}\psi_{\alpha} \right) \right. \right. \\ &\quad \left. \left. + \gamma'N\bar{\psi}_0\bar{\psi}_1\psi_0\psi_1 + \lambda(\bar{\psi}_0\psi_1 + \bar{\psi}_1\psi_0) \right] + O(\tau^2) \right\}. \end{aligned} \quad (33)$$

The orthogonality catastrophe implies that $\langle F|F'\rangle$ vanishes unless $|F\rangle \approx |F'\rangle$, allowing us to set $\psi'_{\alpha} = \psi_{\alpha}$ in the $O(\tau)$ term.

Let $\int D\bar{\psi}_{\alpha} D\psi_{\alpha} \delta(|\psi_0|^2 + |\psi_1|^2 - 1) := \lim_{K \rightarrow \infty} \int (\prod_{k=1}^{K-1} \frac{N+1}{4\pi} \sin \theta_k d\theta_k d\phi_k)$ denote a sum over Bloch sphere paths $\psi_{\alpha}(t_k)$ connecting $|F'\rangle$ to $|F\rangle$, with $t_k = k\tau$. Then we have $\langle F_k|F_{k-1}\rangle = e^{-N\tau \sum_{\alpha} \bar{\psi}_{\alpha}\partial_t \psi_{\alpha} + O(\tau^2)}$ and the propagator can be written in a spin-coherent-state path integral representation as [107]

$$\langle F|e^{-iHt}|F'\rangle = \int D\bar{\psi}_{\alpha} D\psi_{\alpha} \delta(|\psi_0|^2 + |\psi_1|^2 - 1) e^{iS}, \quad S = \int dt \langle F|i\partial_t - H|F\rangle, \quad (34)$$

where

$$S = N \int dt \left\{ \sum_{\alpha=0,1} \left(\bar{\psi}_{\alpha} i\partial_t \psi_{\alpha} - \frac{\omega_{\alpha}}{2} |\psi_{\alpha}|^2 - \gamma_{\alpha}N |\psi_{\alpha}|^4 \right) - \gamma'N |\psi_0\psi_1|^2 - \lambda(\bar{\psi}_0\psi_1 + \bar{\psi}_1\psi_0) \right\}. \quad (35)$$

We assume that the limits $K_{\alpha} = \lim_{N \rightarrow \infty} N\gamma_{\alpha}$ and $K' = \lim_{N \rightarrow \infty} N\gamma'$ exist. Then in the large N limit the stationary phase equations are

$$i \frac{d\psi_0}{dt} = \left(\frac{\omega_0}{2} + 2K_0|\psi_0|^2 + K'|\psi_1|^2 \right) \psi_0 + \lambda\psi_1, \quad (36)$$

$$i \frac{d\psi_1}{dt} = \left(\frac{\omega_1}{2} + 2K_1|\psi_1|^2 + K'|\psi_0|^2 \right) \psi_1 + \lambda\psi_0, \quad (37)$$

as well as their complex conjugates. Therefore we have

$$\frac{d}{dt} \begin{pmatrix} \psi_0 \\ \psi_1 \end{pmatrix} = -iH_{\text{eff}} \begin{pmatrix} \psi_0 \\ \psi_1 \end{pmatrix}, \quad (38)$$

where

$$H_{\text{eff}} = \begin{pmatrix} \frac{\omega_0}{2} + 2K_0|\psi_0|^2 + K'|\psi_1|^2 & \lambda \\ \lambda & \frac{\omega_1}{2} + 2K_1|\psi_1|^2 + K'|\psi_0|^2 \end{pmatrix} \quad (39)$$

$$= B_x \begin{pmatrix} 0 & 1 \\ 1 & 0 \end{pmatrix} + B_z \begin{pmatrix} 1 & 0 \\ 0 & -1 \end{pmatrix} + g(|\psi_0|^2 - |\psi_1|^2) \begin{pmatrix} 1 & 0 \\ 0 & -1 \end{pmatrix} \quad (40)$$

$$+ \left[\frac{\omega_0 + \omega_1}{4} + \frac{K_0 + K_1 + K'}{2} + (|\psi_0|^2 - |\psi_1|^2) \frac{K_0 - K_1}{2} \right] \begin{pmatrix} 1 & 0 \\ 0 & 1 \end{pmatrix} \quad (41)$$

$$= B_x \sigma^x + B_z \sigma^z + g \text{tr}(\rho \sigma^z) \sigma^z + \text{const.}, \quad (42)$$

with

$$B_x := \lambda, \quad B_z := \frac{\omega_0 - \omega_1}{4} + \frac{K_0 - K_1}{2}, \quad g := \frac{K_0 + K_1 - K'}{2}. \quad (43)$$

This Hamiltonian correctly generates the qubit evolution, but the total energy also includes a “background” energy term common to mean field theory:

$$H_{\text{tot}} = H_{\text{eff}} + \Delta E, \quad \Delta E = -\frac{g}{2} [\text{tr}(\rho \sigma^z)]^2. \quad (44)$$

For example, consider a spin model $H_{\text{spin}} = \frac{g}{N} \sum_{1 \leq i < j \leq N} \sigma_i^z \sigma_j^z$ with all-to-all interaction. Expanding $H_{\text{spin}} = H_{\text{lin}} + H_{\text{quad}}$ in powers of fluctuations $\sigma_i^z - \langle \sigma^z \rangle$ and assuming a homogeneous order parameter $\langle \sigma^z \rangle$, and $N \gg 1$, leads to $H_{\text{lin}} = g \sum_{i=1}^N [\langle \sigma^z \rangle \sigma_i^z - \frac{1}{2} \langle \sigma^z \rangle^2]$. In the mean field approximation H_{quad} is neglected and

$$H_{\text{spin}} \approx N[g\langle \sigma^z \rangle \sigma^z - \frac{g}{2} \langle \sigma^z \rangle^2] = N[H_{\text{eff}} - \frac{g}{2} \langle \sigma^z \rangle^2]. \quad (45)$$

3 Single-input state discrimination

3.1 Torsion and conservation laws

To implement nonlinear state discrimination, we consider the symmetric setting $\omega_{0,1} = \omega$ and $K_{0,1} = K$ in (42), which leads to the pure state torsion model (15) plus a σ^x term:

$$H_{\text{eff}} = B_x \sigma^x + g(|\psi_0|^2 - |\psi_1|^2) \sigma^z, \quad g = \frac{2K - K'}{2}. \quad (46)$$

Then in the Pauli basis $r^\mu = \text{tr}(\rho \sigma^\mu)$ and $\frac{dr^\mu}{dt} = -i \text{tr}(\rho [\sigma^\mu, H_{\text{eff}}])$, the model (46) takes the form

$$\frac{dx}{dt} = -2gyz, \quad (47)$$

$$\frac{dy}{dt} = 2gxz - 2B_x z, \quad (48)$$

$$\frac{dz}{dt} = 2B_x y. \quad (49)$$

These equations will be used to design single-input QSD gates. The solutions to these equations when $B_x = 0$ are shown in Figure 2.

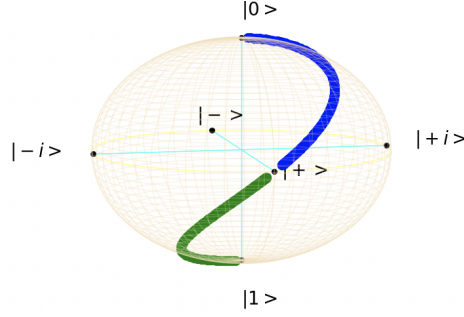


Figure 3: Viviani curve mapping $|a\rangle \mapsto |0\rangle$ (blue) and $|b\rangle \mapsto |1\rangle$ (green).

A single-input QSD gate assumes a given set of potential inputs $\{|a\rangle, |b\rangle\}$ as initial conditions, and the objective is to send $|a\rangle \mapsto |0\rangle$ and $|b\rangle \mapsto |1\rangle$. Thus we are faced with a control problem on the Bloch sphere. A unitary can always be used to orient the pair $\{\vec{r}_a, \vec{r}_b\}$ anywhere on the Bloch sphere without changing the angle between them. Childs and Young (CY) [23] constructed a gate by maximally increasing the trace distance $\|\rho_a - \rho_b\|_1 = |\vec{r}_a - \vec{r}_b|$ until $|\vec{r}'_a - \vec{r}'_b| = 2$ (their Bloch vectors become antiparallel), after which a unitary $U_{\text{read}} = |0\rangle\langle a'| + |1\rangle\langle b'|$ is applied prior to measurement in the $\{|0\rangle, |1\rangle\}$ basis. This leads to a fast gate but requires a time-dependent B_x . Here we take a different approach using a time-independent B_x and no readout unitary.

The Bloch coordinates in the torsion model (47) - (49) satisfy two conservation laws. The first is conservation of total energy (44):

$$E = B_x x + \frac{g}{2} z^2, \quad \frac{dE}{dt} = B_x \frac{dx}{dt} + g z \frac{dz}{dt} = 0. \quad (50)$$

Here we have assumed that B_x and g are constant. The second is conservation of the Bloch vector length (hence purity and entropy):

$$r^2 = x^2 + y^2 + z^2, \quad \frac{dr^2}{dt} = 2x \frac{dx}{dt} + 2y \frac{dy}{dt} + 2z \frac{dz}{dt} = 0. \quad (51)$$

3.2 State discrimination along Viviani's curve

Setting $E = B_x = \frac{g}{2}$ leads to striking orbits in the shape of Viviani's curve, shown in Figure 3, at the intersection of a cylinder (oriented in the z direction) and the Bloch sphere. To understand why, note that when $E = B_x = \frac{g}{2}$ the energy conservation equation for a pure state ($r = 1$) is $x + z^2 = 1 = x^2 + y^2 + z^2$, or $x^2 - x + y^2 = 0$, which is the equation for a cylinder of radius $\frac{1}{2}$ tangent to the Bloch sphere at the state $\vec{r} = (1, 0, 0)$:

$$(x - \frac{1}{2})^2 + y^2 = (\frac{1}{2})^2. \quad (52)$$

Thus we seek an orbit in the shape of Viviani's curve:

$$x = \cos^2 \xi, \quad y = \cos \xi \sin \xi, \quad z = \sin \xi, \quad -\frac{\pi}{2} \leq \xi \leq \frac{\pi}{2}. \quad (53)$$

Note that (53) satisfies (49) if the state traverses the curve with ξ evolving as

$$\xi(t) = 2 \arctan \left[\tan \left(\frac{\xi(0)}{2} \right) e^{2B_x t} \right], \quad \frac{d\xi}{dt} = 2B_x \sin \xi. \quad (54)$$

Also note that (53) satisfies (47) and (48) if $B_x = \frac{g}{2}$. As in the CY gate [23], qubit states $\{|a\rangle, |b\rangle\}$ are initialized to Bloch coordinates

$$x_a = x_b = \left| \cos\left(\frac{\theta_{ab}}{2}\right) \right|, \quad y_a = z_a = \frac{\sin\left(\frac{\theta_{ab}}{2}\right)}{\sqrt{2}}, \quad y_b = z_b = -\frac{\sin\left(\frac{\theta_{ab}}{2}\right)}{\sqrt{2}}, \quad 0 \leq \theta_{ab} \leq \pi, \quad (55)$$

where θ_{ab} is the initial angle between the Bloch vectors \vec{r}_a and \vec{r}_b . For small initial θ_{ab} , the Bloch vectors $\vec{r}_{a,b}$ lie on Viviani's curve with $\xi(0) = \pm(\frac{\theta_{ab}}{2\sqrt{2}})$, where the $+$ ($-$) sign applies to \vec{r}_a (\vec{r}_b). Subsequent evolution of \vec{r}_a follows the Viviani curve ending at classical state $|0\rangle$ where $\xi = \frac{\pi}{2}$ (the blue curve in Figure 3). This occurs after a time

$$t_V = \frac{1}{g} \log \cot\left(\frac{\theta_{ab}}{4\sqrt{2}}\right) \approx \frac{1}{g} \log\left(\frac{4\sqrt{2}}{\theta_{ab}}\right), \quad (56)$$

where the second expression assumes $\theta_{ab} \ll 1$. Similarly, \vec{r}_b follows the Viviani curve down to $|1\rangle$ at $\xi = -\frac{\pi}{2}$ (the green curve). The Viviani gate is efficient in the sense that an exponentially small $\theta_{ab} = 2^{-k}$ takes time $t_V = O(k)/g$.

3.3 Kitagawa-Ueda model as $N \rightarrow \infty$

Bloch sphere torsion provides a quantum information processing advantage by circumventing trace distance monotonicity (13) and enabling expansive qubit dynamics. How do we know this is a real effect and not an artifact of the stationary phase approximation or mean field theory? In the remainder of this section we show that the dynamics of pure torsion ($B_x=0$) shown in Figure 2 follows directly from the exactly solvable Kitagawa-Ueda spin model (25) in the double limit $N \rightarrow \infty$, $\chi \rightarrow 0$. In this model the angular momentum is carried by N two-component atomic qubits

$$J_\mu = \sum_{i=1}^N \frac{\sigma_i^\mu}{2}, \quad \mu \in \{x, y, z\}, \quad (57)$$

instead of the boson fields as in (20). It's possible to calculate $\langle J_\mu \rangle$ as a function of time in the Kitagawa-Ueda model, starting in any N -qubit permutation-symmetric product state $|\Psi_N\rangle = |\psi\rangle^{\otimes N}$, where $|\psi\rangle$ is a single-qubit state. From (30) we obtain

$$\langle J_+ \rangle = \langle \Psi_N | U^\dagger (J_x + iJ_y) U | \Psi_N \rangle = \langle \Psi_N | J_+ e^{2i\chi t J_z} e^{i\chi t} | \Psi_N \rangle, \quad U = e^{-i\chi t J_z^2}. \quad (58)$$

Using (57) then leads to

$$\langle J_+ \rangle = \frac{N}{2} e^{i\chi t} \langle \psi | (\sigma^x + i\sigma^y) e^{i\chi t \sigma^z} | \psi \rangle [\langle \psi | e^{i\chi t \sigma^z} | \psi \rangle]^{N-1} \quad (59)$$

$$= \frac{N}{2} (x + iy) [\cos(\chi t) + iz \sin(\chi t)]^{N-1}. \quad (60)$$

Here x, y, z are the Bloch coordinates of the *initial* single-qubit state $|\psi\rangle$. In addition,

$$\langle J_z \rangle = \frac{N}{2} z, \quad (61)$$

because J_z commutes with the Hamiltonian (25).

Next we take the double limit $N \rightarrow \infty$, $\chi \rightarrow 2g/N$, with g constant [the factor of two comes from (24) and (43)]. The technical part of the calculation is to evaluate

$$f(t) := \lim_{N \rightarrow \infty} \left[\cos\left(\frac{2gt}{N}\right) + iz \sin\left(\frac{2gt}{N}\right) \right]^{N-1}. \quad (62)$$

To do this, rewrite it as $f(t) = \lim_{N \rightarrow \infty} [c_N(t)]^{N-1}$, where $c_N(t) = \cos\left(\frac{2gt}{N}\right) + iz \sin\left(\frac{2gt}{N}\right)$. Then expand $f(t) = f(0) + \sum_{k=1}^{\infty} \frac{t^k}{k!} f^{(k)}(0)$ as a Maclaurin series in time, with $f^{(k)}(t) := \frac{d^k f}{dt^k}$. Note that

$$\frac{df}{dt} = \lim_{N \rightarrow \infty} (N-1)(c_N)^{N-2} \frac{dc_N}{dt}, \quad \frac{dc_N}{dt} = \left[-\sin\left(\frac{2gt}{N}\right) + iz \cos\left(\frac{2gt}{N}\right) \right] \frac{2g}{N}, \quad (63)$$

and

$$\frac{d^2 f}{dt^2} = \lim_{N \rightarrow \infty} \left[(N-1)(N-2)(c_N)^{N-3} \left(\frac{dc_N}{dt} \right)^2 + (N-1)(c_N)^{N-2} \frac{d^2 c_N}{dt^2} \right]. \quad (64)$$

Because $\frac{d^k c_N}{dt^k} = O(N^{-k})$, we see that $\left(\frac{dc_N}{dt}\right)^2$ and $\frac{d^2 c_N}{dt^2}$ are of the same order, so the first term in (64) determines the large N limit. This behavior extends to the higher order derivatives: $\frac{d^k f}{dt^k} = \lim_{N \rightarrow \infty} N^k (c_N)^{N-k-1} \left(\frac{dc_N}{dt}\right)^k$ and $f^{(k)}(0) = N^k \left(\frac{2igz}{N}\right)^k = (2igz)^k$. Therefore we obtain $f(t) = e^{2igzt}$ and

$$\lim_{N \rightarrow \infty} \frac{\langle J_x \rangle}{N/2} = x \cos(2gzt) - y \sin(2gzt), \quad (65)$$

$$\lim_{N \rightarrow \infty} \frac{\langle J_y \rangle}{N/2} = x \sin(2gzt) + y \cos(2gzt), \quad (66)$$

$$\lim_{N \rightarrow \infty} \frac{\langle J_z \rangle}{N/2} = z. \quad (67)$$

To interpret this result, define a vector $\vec{R} = (R_x, R_y, R_z)$ from the normalized angular momentum components $R_\mu := \lim_{N \rightarrow \infty} \frac{\langle J_\mu \rangle}{N/2}$, $\mu \in \{x, y, z\}$, and note that $|\vec{R}(t)| = 1$ and $\vec{R}(0) = (x, y, z)$, where x, y, z are the Bloch vector components of the initial qubit state. Then we find

$$\begin{pmatrix} R_x \\ R_y \\ R_z \end{pmatrix} = \begin{pmatrix} \cos(2gzt) & -\sin(2gzt) & 0 \\ \sin(2gzt) & \cos(2gzt) & 0 \\ 0 & 0 & 1 \end{pmatrix} \begin{pmatrix} R_x \\ R_y \\ R_z \end{pmatrix}_{t=0}. \quad (68)$$

The matrix implements z -axis torsion: A z rotation by angle $2gzt$ proportional to z .

4 Fast discrimination with torsion and dissipation

4.1 Combining contractive and expansive dynamics

The appeal of nonlinear quantum state discrimination based on the CY or Viviani gate is that, assuming knowledge of $|a\rangle$ and $|b\rangle$, a protocol can be designed to implement perfect QSD without multiple copies of the input. However the input $\mathbf{r} \in \{\mathbf{r}_a, \mathbf{r}_b\}$ must be free of errors (in this section we generalize to mixed states described by Bloch vectors). In previous work [38] we considered the combined effects of torsion and dissipation, and investigated a discriminator based on the generation of two basins of attraction $\mathbb{V}_+, \mathbb{V}_- \subset \mathbb{B}$ within the Bloch ball \mathbb{B} , flowing to opposing stable fixed points denoted by Bloch vectors $\{\mathbf{r}_+^{\text{fp}}, \mathbf{r}_-^{\text{fp}}\}$. The nonoverlapping subsets \mathbb{V}_\pm share a two-dimensional boundary cutting through the center of the Bloch ball, across which the discriminator inputs $\{\mathbf{r}_a, \mathbf{r}_b\}$ are placed. The fixed points $\{\mathbf{r}_+^{\text{fp}}, \mathbf{r}_-^{\text{fp}}\}$ are the discriminator outputs. This dynamics leads to an intrinsic tolerance to errors in the input $\mathbf{r} \in \{\mathbf{r}_a, \mathbf{r}_b\}$ that do not cross the boundary into the wrong basin [38]. The gate combines contractive dynamics within the basins of attraction \mathbb{V}_\pm , made possible by the dissipation, with expansive dynamics at their boundary separatrix made possible by the torsion.

Here we develop this idea further, focusing on a related computational benefit of the nonlinear dynamics: autonomy. By this we mean that the discrimination gate and experimental protocol do not depend on the values of $\{\mathbf{r}_a, \mathbf{r}_b\}$, and their prior knowledge is no longer required. In particular, we design an *autonomous* quantum state discrimination gate that distinguishes any state in subset \mathbb{V}_+ from any in \mathbb{V}_- , where \mathbb{V}_\pm are the sets of inputs (basins of attraction) feeding the stable fixed points $\mathbf{r}_\pm^{\text{fp}}$.

Let's put nonlinearity aside briefly and recall how dissipation and decoherence are included in the Bloch sphere picture

$$r^\mu = \text{tr}(\rho\sigma^\mu), \quad \frac{dr^\mu}{dt} = \text{tr}\left(\frac{d\rho}{dt}\sigma^\mu\right), \quad (69)$$

where $\mu \in \{x, y, z\}$. The most general linear time-local equation of motion (linear Markovian master equation) for a quantum state $\rho \in \mathbb{C}^{d \times d}$ is

$$\frac{d\rho}{dt} = -i[H, \rho] + \sum_\alpha \zeta_\alpha B_\alpha \rho B_\alpha^\dagger + \{L_+, \rho\}, \quad L_+ := -\frac{1}{2} \sum_\alpha \zeta_\alpha B_\alpha^\dagger B_\alpha. \quad (70)$$

Here $H \in \mathbb{C}^{d \times d}$ is a Hermitian operator generating unitary evolution, the $B_\alpha \in \mathbb{C}^{d \times d}$ are linear but otherwise arbitrary jump operators generating dissipative and decohering processes, and the $\{L_+, \rho\}$ term conserves the trace of ρ .

The arbitrary signs $\zeta_\alpha \in \pm 1$ determine the degree of positivity preserved by the dynamics: If all $\zeta_\alpha = 1$, then (70) reduces to the Gorini-Kossakowski-Sudarshan-Lindblad equation [96, 97] and the equation of motion generates a completely positive trace-preserving (CPTP) channel [108, 109]. If one or more ζ_α are negative, the map is either positive but not completely positive [110–114], or else it fails to preserve positivity altogether (this is determined by a competition between terms with positive and negative ζ_α). In this paper we are concerned with both positive trace-preserving (PTP) channels [115] and CPTP channels. Substituting (70) with dimension $d = 2$ into (69) yields $\frac{dr^\mu}{dt} = \text{tr}(\sigma^\mu[-iH, \rho] + \sum_\alpha \zeta_\alpha \sigma^\mu B_\alpha \rho B_\alpha^\dagger + \sigma^\mu \{L_+, \rho\})$. Using $\rho = \frac{I_2 + r^\nu \sigma^\nu}{2}$ then leads to

$$\frac{dr^\mu}{dt} = G^{\mu\nu} r^\nu + C^\mu, \quad (71)$$

where

$$G^{\mu\nu} = -\epsilon^{\mu\nu\lambda} \text{tr}(H\sigma^\lambda) + \sum_\alpha \frac{\zeta_\alpha}{2} \text{tr}(\sigma^\mu B_\alpha \sigma^\nu B_\alpha^\dagger) + \text{tr}(L_+) \delta^{\mu\nu} \quad (72)$$

and

$$C^\mu = \sum_\alpha \frac{\zeta_\alpha}{2} \text{tr}(\sigma^\mu [B_\alpha, B_\alpha^\dagger]). \quad (73)$$

4.2 Jump operators

Next we define our dissipation model by specifying a set $\{B_\alpha\}_{\alpha=1}^7$ of single-qubit jump operators. The dissipative torsion model in [38] contains two independently controlled nonunitary processes. The first is depolarization, requiring three jump operators. The second is a non-CP (meaning PTP but not CPTP) process detailed below, requiring four more. Therefore we need seven jump operators in total, which are given in Table 1. The signs ζ_α are also given. The jump operators used here are Hermitian so C^μ vanishes and the channel is unital ($\mathbf{r}=0$ is a fixed point).

α	ζ_α	B_α	$B_\alpha^\dagger B_\alpha$	$\frac{1}{2}\text{tr}(\sigma^\mu B_\alpha \sigma^\nu B_\alpha^\dagger)$
1	+1	$\frac{\sqrt{\gamma}}{2}\sigma^x$	$\frac{\gamma}{4}I_2$	$\gamma \begin{pmatrix} \frac{1}{4} & 0 & 0 \\ 0 & -\frac{1}{4} & 0 \\ 0 & 0 & -\frac{1}{4} \end{pmatrix}$
2	+1	$\frac{\sqrt{\gamma}}{2}\sigma^y$	$\frac{\gamma}{4}I_2$	$\gamma \begin{pmatrix} -\frac{1}{4} & 0 & 0 \\ 0 & \frac{1}{4} & 0 \\ 0 & 0 & -\frac{1}{4} \end{pmatrix}$
3	+1	$\frac{\sqrt{\gamma}}{2}\sigma^z$	$\frac{\gamma}{4}I_2$	$\gamma \begin{pmatrix} -\frac{1}{4} & 0 & 0 \\ 0 & -\frac{1}{4} & 0 \\ 0 & 0 & \frac{1}{4} \end{pmatrix}$
4	+1	$\sqrt{\frac{m}{8}}(\sigma^x + \sigma^y + \sigma^z)$	$\frac{3m}{8}I_2$	$m \begin{pmatrix} -\frac{1}{8} & \frac{1}{4} & \frac{1}{4} \\ \frac{1}{4} & -\frac{1}{8} & \frac{1}{4} \\ \frac{1}{4} & \frac{1}{4} & -\frac{1}{8} \end{pmatrix}$
5	+1	$\sqrt{\frac{m}{8}}(\sigma^x - \sigma^y + \sigma^z)$	$\frac{3m}{8}I_2$	$m \begin{pmatrix} -\frac{1}{8} & -\frac{1}{4} & \frac{1}{4} \\ -\frac{1}{4} & -\frac{1}{8} & -\frac{1}{4} \\ \frac{1}{4} & -\frac{1}{4} & -\frac{1}{8} \end{pmatrix}$
6	-1	$\sqrt{\frac{m}{8}}(\sigma^x + \sigma^y - \sigma^z)$	$\frac{3m}{8}I_2$	$m \begin{pmatrix} -\frac{1}{8} & \frac{1}{4} & -\frac{1}{4} \\ \frac{1}{4} & -\frac{1}{8} & -\frac{1}{4} \\ -\frac{1}{4} & -\frac{1}{4} & -\frac{1}{8} \end{pmatrix}$
7	-1	$\sqrt{\frac{m}{8}}(\sigma^x - \sigma^y - \sigma^z)$	$\frac{3m}{8}I_2$	$m \begin{pmatrix} -\frac{1}{8} & -\frac{1}{4} & -\frac{1}{4} \\ -\frac{1}{4} & -\frac{1}{8} & \frac{1}{4} \\ -\frac{1}{4} & \frac{1}{4} & -\frac{1}{8} \end{pmatrix}$

Table 1: Jump operators used in the dissipative torsion model. The dimensionless model parameters γ, m are real and nonnegative. I_2 is the two-dimensional identity.

Using the jump operators defined in Table 1, we obtain

$$L_+ = -\frac{1}{2} \sum_{\alpha} \zeta_{\alpha} B_{\alpha}^{\dagger} B_{\alpha} = -\frac{3\gamma}{8} I_2 \quad \text{and} \quad \text{tr}(L_+) = -\frac{3\gamma}{4}. \quad (74)$$

Having specified the linear model, we now include nonlinearity by using the state-dependent torsion Hamiltonian (15) in the first term of (72). This leads to a nonlinear (z dependent) Pauli basis generator

$$G = m \lambda_4 - \gamma I_3 + 2gz E_z, \quad (75)$$

where

$$\lambda_4 = \begin{pmatrix} 0 & 0 & 1 \\ 0 & 0 & 0 \\ 1 & 0 & 0 \end{pmatrix} \quad \text{and} \quad E_z = \begin{pmatrix} 0 & -1 & 0 \\ 1 & 0 & 0 \\ 0 & 0 & 0 \end{pmatrix}. \quad (76)$$

Here λ_4 is an SU(3) generator, I_3 is the three-dimensional identity, and E_z is an SO(3) generator. Dimensionless parameters γ, m are real and nonnegative. Instead of (47)-(49), we now have

$$\frac{dx}{dt} = mz - \gamma x - 2gyz, \quad (77)$$

$$\frac{dy}{dt} = -\gamma y + 2gxz, \quad (78)$$

$$\frac{dz}{dt} = mx - \gamma z. \quad (79)$$

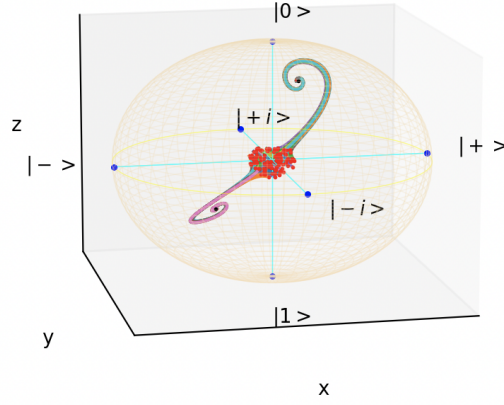


Figure 4: Curves show solutions of qubit equations of motion (77)-(79) for 100 random initial conditions (uniformly distributed within a ball of radius 0.15), shown as red points. Blue points mark pure states on the x, y, z axes. Black dots are the fixed points (84). Model parameters are $\gamma = 0.5$, $m = 1$, and $g = 0.8$. In addition, $\delta = 0.75$ and $g_{\min} = 0.612$.

4.3 Fixed points

The fixed-point equations for the dissipative torsion model are

$$mz - \gamma x - 2gyz = 0, \quad -\gamma y + 2gxz = 0, \quad mx - \gamma z = 0. \quad (80)$$

The origin $\mathbf{r}_0^{\text{fp}} = (0, 0, 0)$ is a fixed point (the channel is unital), although not always stable.

If $g = 0$, all fixed points must be confined to the $y = 0$ plane. Beyond \mathbf{r}_0^{fp} , there are no additional fixed points unless $\gamma = m$, in which case there is a continuum of fixed points on the line $\mathbf{r}_{z=x} = \{(w, 0, w) : w \in \mathbb{R}\}$. The setting $\gamma = m$ is a singularity in the parameter space of the linearized model. Controlling this singularity in the presence of nonlinearity is the key to autonomous QSD.

Next we discuss the fixed points $\mathbf{r}_{\pm}^{\text{fp}}$ and their basins of attraction \mathbb{V}_{\pm} . We have seen that $\mathbf{r}_0^{\text{fp}} = (0, 0, 0)$ is a fixed point. Are there more? Assuming $g > 0$, $m > 0$, $\gamma > 0$, $\mathbf{r} \neq 0$, and eliminating z , the fixed point conditions are

$$m^2 - \gamma^2 = 2gmy, \quad (81)$$

$$\gamma^2 y = 2gm x^2. \quad (82)$$

Thus, any additional fixed points must be confined to the plane

$$y = \frac{m^2 - \gamma^2}{2gm}. \quad (83)$$

However (82) requires $y \geq 0$, which is only possible when $m^2 \geq \gamma^2$. Therefore, when $m^2 < \gamma^2$, the only fixed point is \mathbf{r}_0^{fp} (and this is stable for all $m^2 < \gamma^2$). But if $m > \gamma$, the fixed point \mathbf{r}_0^{fp} is unstable and there is a new pair of stable fixed points at

$$\mathbf{r}_{\pm}^{\text{fp}} = \left(\pm \frac{\gamma}{2g} \sqrt{\delta}, \frac{m}{2g} \delta, \pm \frac{m}{2g} \sqrt{\delta} \right), \quad \delta := \frac{m^2 - \gamma^2}{m^2} \geq 0. \quad (84)$$

For these to be contained within the Bloch sphere requires $g \geq g_{\min}$, where

$$g_{\min} = \sqrt{\frac{m^2 - \gamma^2}{2}}. \quad (85)$$

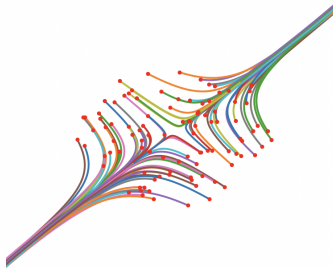


Figure 5: Expanded view of Figure 4, seen from the y direction, exposing the boundary separatrix between \mathbb{V}_- and \mathbb{V}_+ . Model parameters are $\gamma = 0.5$, $m = 1$, and $g = 0.8$.

4.4 Autonomous state discrimination

The autonomous QSD gate operates by placing the discriminator inputs $\{\mathbf{r}_a, \mathbf{r}_b\}$ exponentially close to the origin but flowing to different fixed points. Figure 4 shows the Bloch sphere together with the simulated evolution of random initial states (within a small radius and indicated by red dots) flowing to the discriminator outputs $\mathbf{r}_\pm^{\text{fp}}$ (black dots). To obtain the basins of attraction \mathbb{V}_\pm , examine the equations close to the origin, where $|\mathbf{r}| \ll 1/g$ and the nonlinearity can be neglected. In this limit the y motion is decoupled from x and z [see (78)], and it is always stable for $\gamma > 0$. The x and z motion is simplest in rotated coordinates $\xi_\pm = (z \pm x)/2$, where

$$\frac{d\xi_+}{dt} = (m - \gamma)\xi_+ \quad \text{and} \quad \frac{d\xi_-}{dt} = -(m + \gamma)\xi_-. \quad (86)$$

The ξ_+ and ξ_- variables are also decoupled in the linearized model. ξ_+ is the coordinate along the line $z = x$ (and $y = 0$), and ξ_- is the coordinate along the perpendicular line $z = -x$. Motion in the ξ_- direction is always stable. However the ξ_+ motion is unstable here because $m > \gamma$. Let $\mathbb{E}^2 = \{(x, y, z) \in \mathbb{R}^3 : x + z = 0\}$ be the two-dimensional plane separating half-spaces $\xi_+ < 0$ and $\xi_+ > 0$. When $g = 0$, the plane \mathbb{E}^2 separates \mathbb{V}_- (where $\xi_+ < 0$) and \mathbb{V}_+ (where $\xi_+ > 0$): it is the separatrix in the linearized model. In the nonlinear model, the separatrix is a non-planar surface, but in the region of interest near the origin the separatrix coincides with \mathbb{E}^2 . Therefore \mathbb{E}^2 can be used as a surface across which the discriminator inputs $\{\mathbf{r}_a, \mathbf{r}_b\}$ are prepared. Figure 5 shows the evolution of states initialized close to the plane \mathbb{E}^2 , separating the basins of attraction \mathbb{V}_- and \mathbb{V}_+ .

The autonomous QSD gate discussed here is no longer a single-input protocol because the outputs $\mathbf{r}_\pm^{\text{fp}}$ are not perfectly distinguishable. However, because the fixed points $\mathbf{r}_\pm^{\text{fp}}$ are known explicitly [see (84)], we expect that a second step mapping them to the perfectly distinguishable classical states $\{|0\rangle, |1\rangle\}$ can be implemented, making the gate both single-input and autonomous (we do not discuss the second step here).

5 Discussion

In standard gate-based quantum computation, a register of qubits is initialized to a product state, such as $|0\rangle^{\otimes N}$, after which gates (linear CPTP channels) are applied, entangling the qubits. In the nonlinear approach discussed here, a register of bosonic qubits is initialized into a symmetric product state through condensation and subsequently controlled by varying the qubit-qubit interaction. Entanglement is suppressed by making N large and interaction weak, so the qubits ideally remain in a product state $|\psi(t)\rangle^{\otimes N}$ throughout the computation. The N atoms simulate a single nonlinear qubit.

We considered setups for a two-component BEC to implement a nonlinear qubit with torsion (one-axis twisting). Torsion is computationally powerful because it violates trace-distance monotonicity and allows a pair of states to become more distinguishable. Our work builds on previous proposals [39, 40] for creating nonlinear qubits, but is likely simpler as it is based on previously established spin-squeezing techniques [4–17].

The nonlinear picture is intriguing, but it is also important to keep in mind its limitations: First, the reduction of 3SAT to QSD requires that the nonlinear qubit be entangled with a scalable, error-corrected quantum computing architecture, such as superconducting qubits [116–118], neutral atom arrays [119, 120], or trapped ions [121, 122]. A promising approach is to couple the BEC to a trapped ion [70–72], building on recent advances combining cold atom magneto-optical traps and optical lattices with electromagnetic traps for ions [63–72]. Second, the ability to implement perfect single-input QSD does not immediately imply the ability to solve 3SAT because we do not know the number of satisfying assignments, s . However with additional assumptions about the action of the gate on states $|\psi\rangle \notin \{|a\rangle, |b\rangle\}$, it is possible to measure s efficiently [22, 29]. Third, the nonlinear approach trades exponential time complexity for space complexity, requiring N (the number of atoms) to be large. Long computations will require N to be exponentially large, eventually limiting scalability. Fourth, long computations will also require error correction. This is an interesting and challenging problem, as existing quantum error correction techniques assume linear quantum mechanics.

Acknowledgements

This work was partly supported by the NSF under grant no. DGE-2152159.

A Entanglement monogamy

In this section we give an elementary derivation of the monogamy inequality (10) for three qubits in a pure state

$$\tau(\rho_{12}) + \tau(\rho_{13}) \leq 4 \det(\rho_1), \quad \rho_1 = \text{tr}_{23}(\rho_{123}), \quad \rho_{123} = |\psi\rangle\langle\psi|, \quad (87)$$

originally proved in [91], but now simplified by the additional assumption of permutation symmetry. Here $\text{tr}_{23}(\cdot)$ denotes partial trace over qubits 2 and 3. Concurrence [123] and tangle (concurrence squared) measure the entanglement in some two-qubit pure or mixed state $\rho_{ij} \in \mathbb{C}^{4 \times 4}$ through a matrix

$$T := \rho_{ij} \tilde{\rho}_{ij}, \quad \tilde{\rho}_{ij} := \sigma^y \otimes \sigma^y \bar{\rho}_{ij} \sigma^y \otimes \sigma^y \quad (88)$$

where $\bar{\rho}_{ij}$ is the complex conjugate of ρ_{ij} in the standard (σ^z eigenstate) basis. Note that the matrix T usually depends on the qubit pair (i, j) considered, but this dependence is suppressed. Concurrence $C(\rho_{ij})$ is defined through the eigenvalues of T , which are nonnegative with square roots λ_i :

$$\text{spec}(T) = \{\lambda_1^2, \lambda_2^2, \lambda_3^2, \lambda_4^2\}, \quad \lambda_1 \geq \lambda_2 \geq \lambda_3 \geq \lambda_4 \geq 0. \quad (89)$$

Then [123]

$$\tau(\rho_{ij}) = C(\rho_{ij})^2, \quad C(\rho_{ij}) = \max\{\Delta, 0\}, \quad \Delta := \lambda_1 - \lambda_2 - \lambda_3 - \lambda_4. \quad (90)$$

Entangled and separable states are divided by a hyperplane $\Delta = 0$ in the space of allowed λ_i . Entangled states live in the open half-space $\Delta > 0$, while separable states (irrelevant

to monogamy) live in the closed half-space $\Delta \leq 0$. However our proof of (87) will require $\Delta \geq 0$, so that $C(\rho_{ij}) = \Delta$. We achieve this requirement by assuming that $\Delta > 0$ until the end of the calculation where the limit $\Delta \rightarrow 0$ can be taken. With this assumption,

$$\tau(\rho_{ij}) = (\lambda_1 - \lambda_2 - \lambda_3 - \lambda_4)^2 \leq \lambda_1^2 + \lambda_2^2 + \lambda_3^2 + \lambda_4^2 = \text{tr}(T). \quad (91)$$

To derive (87), first note that every pure symmetric state of three qubits lies in a 4-dimensional subspace, namely

$$|\psi_s\rangle = a|000\rangle + b|111\rangle + c|W\rangle + d|V\rangle, \quad |a|^2 + |b|^2 + |c|^2 + |d|^2 = 1, \quad (92)$$

where

$$|W\rangle = \frac{|001\rangle + |010\rangle + |100\rangle}{\sqrt{3}} \quad \text{and} \quad |V\rangle = \frac{|011\rangle + |101\rangle + |110\rangle}{\sqrt{3}} \quad (93)$$

are both permutation symmetric. Our derivation will also make use of the following two-qubit states

$$\begin{aligned} |A\rangle &= a|00\rangle + \frac{d}{\sqrt{3}}|11\rangle + \sqrt{\frac{2}{3}}c|\Psi^+\rangle, \\ |B\rangle &= \frac{c}{\sqrt{3}}|00\rangle + b|11\rangle + \sqrt{\frac{2}{3}}d|\Psi^+\rangle, \\ |C\rangle &= \frac{\bar{d}}{\sqrt{3}}|00\rangle + \bar{a}|11\rangle - \sqrt{\frac{2}{3}}\bar{c}|\Psi^+\rangle, \\ |D\rangle &= \bar{b}|00\rangle + \frac{\bar{c}}{\sqrt{3}}|11\rangle - \sqrt{\frac{2}{3}}\bar{d}|\Psi^+\rangle, \end{aligned} \quad (94)$$

where $|\Psi^+\rangle = 2^{-\frac{1}{2}}(|01\rangle + |10\rangle)$ is a Bell state and \bar{z} denotes complex conjugation. A short calculation then shows that

$$\begin{aligned} & |\langle A|C\rangle|^2 + |\langle A|D\rangle|^2 + |\langle B|C\rangle|^2 + |\langle B|D\rangle|^2 \\ &= 2|a|^2|b|^2 + \frac{4}{3}(|a|^2|d|^2 + |b|^2|c|^2) + \frac{2}{9}|c|^2|d|^2 + \frac{4}{9}(|c|^4 + |d|^4) - \frac{4}{3}\text{Re}[ab\bar{c}\bar{d} + \frac{2}{\sqrt{3}}(a\bar{c}^2d + b\bar{c}d^2)] \\ &= 2(|a|^2 + \frac{2}{3}|c|^2 + \frac{1}{3}|d|^2)(|b|^2 + \frac{1}{3}|c|^2 + \frac{2}{3}|d|^2) - 2|\frac{1}{\sqrt{3}}a\bar{c} + \frac{2}{3}c\bar{d} + \frac{1}{\sqrt{3}}\bar{b}d|^2. \end{aligned} \quad (95)$$

To obtain (87) note that

$$\rho_{12} = \text{tr}_3(|\psi_s\rangle\langle\psi_s|) = |A\rangle\langle A| + |B\rangle\langle B| \quad \text{and} \quad \tilde{\rho}_{12} = |C\rangle\langle C| + |D\rangle\langle D|, \quad (96)$$

where $\text{tr}_3(\cdot)$ is partial trace over qubit 3. Furthermore,

$$\rho_1 = \text{tr}_2(\rho_{12}) = \begin{pmatrix} |a|^2 + \frac{2}{3}|c|^2 + \frac{1}{3}|d|^2 & \frac{1}{\sqrt{3}}a\bar{c} + \frac{2}{3}c\bar{d} + \frac{1}{\sqrt{3}}\bar{b}d \\ \frac{1}{\sqrt{3}}\bar{a}c + \frac{2}{3}\bar{c}d + \frac{1}{\sqrt{3}}b\bar{d} & |b|^2 + \frac{1}{3}|c|^2 + \frac{2}{3}|d|^2 \end{pmatrix}. \quad (97)$$

Then

$$\text{tr}(\rho_{12}\tilde{\rho}_{12}) = |\langle A|C\rangle|^2 + |\langle A|D\rangle|^2 + |\langle B|C\rangle|^2 + |\langle B|D\rangle|^2 = 2\det(\rho_1). \quad (98)$$

Using permutation symmetry we also have $\text{tr}(\rho_{13}\tilde{\rho}_{13}) = 2\det(\rho_1)$. Thus, inequality (91) leads to $\tau(\rho_{12}) + \tau(\rho_{13}) \leq \text{tr}(\rho_{12}\tilde{\rho}_{12}) + \text{tr}(\rho_{13}\tilde{\rho}_{13}) = 4\det(\rho_1)$ as required.

Three qubits is the minimum number needed to analyze the sharing of two-qubit entanglement. Coffman, Kundu, and Wootters [91] derived (87) and conjectured that it would generalize to (10) for $N > 3$. This was later proved by Osborne and Verstraete [92], an important milestone in monogamy theory [124, 125]. We do not provide an independent proof for general N , but rely on Osborne and Verstraete [92] for this justification.

B Monotonicity of trace distance

Here we prove the monotonicity of trace distance given above in (13), which governs how the distance between a pair of states can change as they evolve under the same positive trace-preserving (PTP) channel ϕ . The trace norm $\|\cdot\|_1$ is defined in (8). We will also use an equivalent variational characterization of the trace norm on Hermitian operators [98]

$$\|X\|_1 = 2 \max_{0 \preceq E \preceq I} \text{tr}(EX) = 2 \text{tr}(E_\star X), \quad (99)$$

where the maximization is over all positive semidefinite (PSD) operators E with spectrum bounded by unity (such as POVM elements and projectors). In the second expression, $E_\star := \text{argmax}_{0 \preceq E \preceq I} \text{tr}(EX)$ is the optimal E . In addition, the norm of any state is unity: $\|\rho\|_1 = \text{tr}(|\rho\rangle) = \text{tr}(\rho) = 1$. The inequality (13) means that linear PTP channels are either distance-preserving (unitary) or contractive, but never expansive. It expresses the monotonicity of trace distance under PTP maps. Although (13) is a special case of a theorem on the monotonicity of a (generalized) relative entropy [99], we repeat a simpler direct proof [98, 126] here. Given a pair of states ρ and ρ' , let $X = \rho - \rho'$ be a Hermitian operator. Then

$$X = \rho - \rho' = UDU^\dagger = U(D_> - D_<)U^\dagger = X_> - X_<, \quad (100)$$

$$X_> = UD_>U^\dagger, \quad X_< = UD_<U^\dagger, \quad X_>X_< = X_<X_> = 0, \quad (101)$$

where U is unitary, D is diagonal, and where $D_>$ and $D_<$ are diagonal and PSD. Here $D_>$ contains the positive eigenvalues of X and $D_<$ contains the absolute values of the negative eigenvalues. Then

$$\|\rho - \rho'\|_1 = \text{tr}(|X_> - X_<|) = \text{tr}(\sqrt{X_>^2 + X_<^2}) = \text{tr}(X_> + X_<) = \text{tr}[\phi(X_> + X_<)], \quad (102)$$

where the last step follows from trace conservation. Because $\text{tr}(X) = 0$, we have $\text{tr}(X_>) = \text{tr}(X_<)$ and $\text{tr}[\phi(X_>)] = \text{tr}[\phi(X_<)]$. Using this leads to

$$\|\rho - \rho'\|_1 = 2 \text{tr}[\phi(X_>)]. \quad (103)$$

Suppose A and B are positive operators, with the eigenvalues of B bounded by unity: $0 \leq \text{spec}(B) \leq 1$. In the eigenbasis $\{|\phi_\alpha\rangle\}_{\alpha=1}^d$ of B , such that $B|\phi_\alpha\rangle = b_\alpha|\phi_\alpha\rangle$, we have

$$B = \sum_{\alpha} b_{\alpha} |\phi_{\alpha}\rangle\langle\phi_{\alpha}|, \quad 0 \leq b_{\alpha} \leq 1. \quad (104)$$

Evaluating $\text{tr}(A)$ in the B eigenbasis and using $b_\alpha \leq 1$ leads to

$$\text{tr}(A) = \sum_{\alpha} \langle\phi_{\alpha}|A|\phi_{\alpha}\rangle \geq \sum_{\alpha} b_{\alpha} \langle\phi_{\alpha}|A|\phi_{\alpha}\rangle = \text{tr}(AB). \quad (105)$$

Apply this inequality to (103), where for B we choose $B_\star = \text{argmax}_{0 \preceq B \preceq I} \text{tr}(B\phi(\rho - \rho'))$. Then

$$\|\rho - \rho'\|_1 = 2 \text{tr}[\phi(X_>)] \geq 2 \text{tr}[B_\star\phi(X_>)] \geq 2 \text{tr}[B_\star\phi(X_> - X_<)] = \|\phi(\rho - \rho')\|_1, \quad (106)$$

because $\text{tr}[B_\star\phi(X_<)]$ is nonnegative, proving (13).

References

- [1] C. M. Caves, K. S. Thorne, R. W. P. Drever, V. D. Sandberg, and M. Zimmermann. On the measurement of a weak classical force coupled to a quantum-mechanical oscillator. I. Issues of principle. *Rev. Mod. Phys.*, 52:341, 1980. DOI: [10.1103/RevModPhys.52.341](https://doi.org/10.1103/RevModPhys.52.341).
- [2] V. Giovannetti, S. Lloyd, and L. Maccone. Quantum-enhanced measurements: Beating the standard quantum limit. *Science*, 306:1330, 2004. DOI: [10.1126/science.1104149](https://doi.org/10.1126/science.1104149).
- [3] V. Giovannetti, S. Lloyd, and L. Maccone. Quantum metrology. *Phys. Rev. Lett.*, 96:010401, 2006. DOI: [10.1103/PhysRevLett.96.010401](https://doi.org/10.1103/PhysRevLett.96.010401).
- [4] M. Kitagawa and M. Ueda. Squeezed spin states. *Phys. Rev. A*, 47:5138, 1993. DOI: [10.1103/PhysRevA.47.5138](https://doi.org/10.1103/PhysRevA.47.5138).
- [5] J. Hald, J. L. Sørensen, C. Schori, and E. S. Polzik. Spin squeezed atoms: A macroscopic entangled ensemble created by light. *Phys. Rev. Lett.*, 39:1319, 1999. DOI: [10.1103/PhysRevLett.83.1319](https://doi.org/10.1103/PhysRevLett.83.1319).
- [6] A. Kuzmich, L. Mandel, and N. P. Bigelow. Generation of spin squeezing via continuous quantum nondemolition measurement. *Phys. Rev. Lett.*, 85:1594, 2000. DOI: [10.1103/PhysRevLett.85.1594](https://doi.org/10.1103/PhysRevLett.85.1594).
- [7] X. Wang and B. C. Sanders. Spin squeezing and pairwise entanglement for symmetric multiqubit states. *Phys. Rev. A*, 68:012101, 2003. DOI: [10.1103/PhysRevA.68.012101](https://doi.org/10.1103/PhysRevA.68.012101).
- [8] G.-R. Jin and S. W. Kim. Storage of spin squeezing in a two-component Bose-Einstein condensate. *Phys. Rev. Lett.*, 99:170405, 2007. DOI: [10.1103/PhysRevLett.99.170405](https://doi.org/10.1103/PhysRevLett.99.170405).
- [9] J. Ma, X. Wang, C. P. Sun, and F. Nori. Quantum spin squeezing. *Phys. Rep.*, 509:89, 2011. DOI: [10.1016/j.physrep.2011.08.003](https://doi.org/10.1016/j.physrep.2011.08.003).
- [10] C. L. Degen, F. Reinhard, and P. Cappellaro. Quantum sensing. *Rev. Mod. Phys.*, 89:035002, 2017. DOI: [10.1103/RevModPhys.89.035002](https://doi.org/10.1103/RevModPhys.89.035002).
- [11] J. Estève, C. Gross, A. Weller, S. Giovanazzi, and M. K. Oberthaler. Squeezing and entanglement in a Bose-Einstein condensate. *Nature*, 455:1216, 2008. DOI: [10.1038/nature07332](https://doi.org/10.1038/nature07332).
- [12] L. Pezzè, A. Smerzi, M. K. Oberthaler, R. Schmied, and P. Treutlein. Quantum metrology with nonclassical states of atomic ensembles. *Rev. Mod. Phys.*, 90:035005, 2018. DOI: [10.1103/RevModPhys.90.035005](https://doi.org/10.1103/RevModPhys.90.035005).
- [13] X. Chai, D. Lao, K. Fujimoto, R. Hamazaki, M. Ueda, and C. Raman. Magnetic solitons in a spin-1 Bose-Einstein condensate. *Phys. Rev. Lett.*, 125:030402, 2020. DOI: [10.1103/PhysRevLett.125.030402](https://doi.org/10.1103/PhysRevLett.125.030402).
- [14] L. Xin, M. S. Chapman, and T. A. B. Kennedy. Fast generation of time-stationary spin-1 squeezed states by nonadiabatic control. *PRX Quantum*, 3:010328, 2022. DOI: [10.1103/PRXQuantum.3.010328](https://doi.org/10.1103/PRXQuantum.3.010328).
- [15] L. Xin, M. Barrios, J. T. Cohen, and M. S. Chapman. Long-lived squeezed ground states in a quantum spin ensemble. *Phys. Rev. Lett.*, 131:133402, 2023. DOI: [10.1103/PhysRevLett.131.133402](https://doi.org/10.1103/PhysRevLett.131.133402).
- [16] D. Barberena, A. Chu, J. K. Thompson, and A. M. Rey. Trade-offs between unitary and measurement induced spin squeezing in cavity QED. arXiv: 2309.15353.
- [17] C. Luo, H. Zhang, A. Chu, C. Maruko, A. M. Rey, and J. K. Thompson. Hamiltonian engineering of collective XYZ spin models in an optical cavity: From one-axis twisting to two-axis counter twisting models. arXiv: 2402.19429.
- [18] J. M. Radcliffe. Some properties of coherent spin states. *J. Phys. A: Gen. Phys.*, 4:313, 1971. DOI: [10.1088/0305-4470/4/3/009](https://doi.org/10.1088/0305-4470/4/3/009).

- [19] J. I. Cirac, M. Lewenstein, K. Mølmer, and P. Zoller. Quantum superposition states of Bose-Einstein condensates. *Phys. Rev. A*, 57:1208, 1998. DOI: [10.1103/PhysRevA.57.1208](https://doi.org/10.1103/PhysRevA.57.1208).
- [20] T. Byrnes, K. Wen, and Y. Yamamoto. Macroscopic quantum computation using Bose-Einstein condensates. *Phys. Rev. A*, 85:040306(R), 2012. DOI: [10.1103/PhysRevA.85.040306](https://doi.org/10.1103/PhysRevA.85.040306).
- [21] T. Byrnes, D. Rosseau, M. Khosla, A. Pyrkov, A. Thomasen, T. Mukai, S. Koyama, A. Abdelrahman, and E. Ilo-Okeke. Macroscopic quantum information processing using spin coherent states. *Optics Communications*, 337:102, 2015. DOI: [10.1016/j.optcom.2014.08.017](https://doi.org/10.1016/j.optcom.2014.08.017).
- [22] D. S. Abrams and S. Lloyd. Nonlinear quantum mechanics implies polynomial-time solution for NP-Complete and #P problems. *Phys. Rev. Lett.*, 81:3992, Nov 1998. DOI: [10.1103/PhysRevLett.81.3992](https://doi.org/10.1103/PhysRevLett.81.3992). URL <https://link.aps.org/doi/10.1103/PhysRevLett.81.3992>.
- [23] A. M. Childs and J. Young. Optimal state discrimination and unstructured search in nonlinear quantum mechanics. *Phys. Rev. A*, 93:022314, 2016. DOI: [10.1103/PhysRevA.93.022314](https://doi.org/10.1103/PhysRevA.93.022314). URL <https://link.aps.org/doi/10.1103/PhysRevA.93.022314>.
- [24] H. Bechmann-Pasquinucci, B. Huttner, and N. Gisin. Nonlinear quantum state transformation of spin-1/2. *Phys. Lett. A*, 242:198, 1998.
- [25] M. Czachor. Notes on nonlinear quantum algorithms. *Acta Phys. Slov.*, 48:157, 1998.
- [26] M. Czachor. Local modification of the Abrams-Lloyd nonlinear algorithm. [quant-ph/9803019](https://arxiv.org/abs/quant-ph/9803019).
- [27] D. R. Terno. Nonlinear operations in quantum-information theory. *Phys. Rev. A*, 59:3320, 1999. DOI: [10.1103/PhysRevA.59.3320](https://doi.org/10.1103/PhysRevA.59.3320).
- [28] D. Bacon. Quantum computational complexity in the presence of closed timelike curves. *Phys. Rev. A*, 70:032309, Sep 2004. DOI: [10.1103/PhysRevA.70.032309](https://doi.org/10.1103/PhysRevA.70.032309). URL <https://link.aps.org/doi/10.1103/PhysRevA.70.032309>.
- [29] S. Aaronson. NP-complete problems and physical reality. arXiv: [quant-ph/0502072](https://arxiv.org/abs/quant-ph/0502072).
- [30] T. A. Brun, J. Harrington, and M. M. Wilde. Localized closed timelike curves can perfectly distinguish quantum states. *Phys. Rev. Lett.*, 102:210402, 2009. DOI: [10.1103/PhysRevLett.102.210402](https://doi.org/10.1103/PhysRevLett.102.210402). URL <https://link.aps.org/doi/10.1103/PhysRevLett.102.210402>.
- [31] C. H. Bennett, D. Leung, G. Smith, and J. A. Smolin. Can closed timelike curves or nonlinear quantum mechanics improve quantum state discrimination or help solve hard problems? *Phys. Rev. Lett.*, 103:170502, 2009. DOI: [10.1103/PhysRevLett.103.170502](https://doi.org/10.1103/PhysRevLett.103.170502). URL <https://link.aps.org/doi/10.1103/PhysRevLett.103.170502>.
- [32] M. E. Kahou and D. L. Feder. Quantum search with interacting Bose-Einstein condensates. *Phys. Rev. A*, 88:032310, 2013. DOI: [10.1103/PhysRevA.88.032310](https://doi.org/10.1103/PhysRevA.88.032310). URL <https://link.aps.org/doi/10.1103/PhysRevA.88.032310>.
- [33] D. A. Meyer and T. G. Wong. Nonlinear quantum search using the Gross-Pitaevskii equation. *New J. Phys.*, 15:063014, 2013.
- [34] D. A. Meyer and T. G. Wong. Quantum search with general nonlinearities. *Phys. Rev. A*, 89:012312, 2014. DOI: [doi:10.1088/1367-2630/15/6/063014](https://doi.org/10.1088/1367-2630/15/6/063014).
- [35] G. Di Molfetta and B. Herzog. Searching via nonlinear quantum walk on the 2D-grid. arXiv: [2009.07800](https://arxiv.org/abs/2009.07800).
- [36] S. Deffner. Nonlinear speed-ups in ultracold quantum gases. *Europhys. Lett.*, 140:48001, 2022. DOI: [10.1209/0295-5075/ac9fed](https://doi.org/10.1209/0295-5075/ac9fed).

- [37] S. Xu, J. Schmiedmayer, and B. C. Sanders. Nonlinear quantum gates for a Bose-Einstein condensate. *Phys. Rev. Research*, 4:023071, 2022. DOI: [10.1103/PhysRevResearch.4.023071](https://doi.org/10.1103/PhysRevResearch.4.023071).
- [38] M. R. Geller. Fast quantum state discrimination with nonlinear PTP channels. *Adv. Quantum Technol.*, page 2200156, 2023. DOI: [10.1002/qute.202200156](https://doi.org/10.1002/qute.202200156). arXiv: 2111.05977.
- [39] M. R. Geller. Protocol for nonlinear state discrimination in rotating condensate. *Adv. Quantum Technol.*, page 202300431, 2024. DOI: [10.1002/qute.202300431](https://doi.org/10.1002/qute.202300431). arXiv: 2404.16288.
- [40] A. GroBardt. Nonlinear-ancilla aided quantum algorithm for nonlinear Schrödinger equations. arXiv: 2403.10102.
- [41] S. M. Barnett and S. Croke. Quantum state discrimination. arXiv: 0810.1970.
- [42] J. Bae and W.-Y. Hwang. Minimum-error discrimination of qubit states: Methods, solutions, and properties. *Phys. Rev. A*, 87:012334, 2013. DOI: [10.1103/PhysRevA.87.012334](https://doi.org/10.1103/PhysRevA.87.012334).
- [43] J. Bae and L.-C. Kwek. Quantum state discrimination and its applications. *J. Phys. A: Math. Theor.*, 48:083001, 2015. DOI: [10.1088/1751-8113/48/8/083001](https://doi.org/10.1088/1751-8113/48/8/083001).
- [44] M. Rouhbakhsh and S. A. Ghoreishi. Minimum-error discrimination of qubit states revisited. arXiv: 2108.12299.
- [45] S. Arora and B. Barak. *Computational Complexity: A Modern Approach*. Cambridge University Press, 2009.
- [46] C. G. Shull, D. K. Atwood, J. Arthur, and M. A. Horne. Search for a nonlinear variant of the Schrödinger equation by neutron interferometry. *Phys. Rev. Lett.*, 44:765, 1980. DOI: [10.1103/PhysRevLett.44.765](https://doi.org/10.1103/PhysRevLett.44.765).
- [47] R. Gähler, A. G. Klein, and A. Zeilinger. Neutron optical tests of nonlinear wave mechanics. *Phys. Rev. A*, 23:1611, 1981. DOI: [10.1103/PhysRevA.23.1611](https://doi.org/10.1103/PhysRevA.23.1611).
- [48] S. Weinberg. Precision tests of quantum mechanics. *Phys. Rev. Lett.*, 62:485, 1989. DOI: [10.1103/PhysRevLett.62.485](https://doi.org/10.1103/PhysRevLett.62.485). URL <https://link.aps.org/doi/10.1103/PhysRevLett.62.485>.
- [49] J. J. Bollinger, D. J. Heinzen, W. M. Itano, S. L. Gilbert, and D. J. Wineland. Test of the linearity of quantum mechanics by rf spectroscopy of the ${}^9\text{Be}^+$ ground state. *Phys. Rev. Lett.*, 63:1031, 1989. DOI: [10.1103/PhysRevLett.63.1031](https://doi.org/10.1103/PhysRevLett.63.1031). URL <https://link.aps.org/doi/10.1103/PhysRevLett.63.1031>.
- [50] T. E. Chupp and R. J. Hoare. Coherence in freely precessing ${}^{21}\text{Ne}$ and a test of linearity of quantum mechanics. *Phys. Rev. Lett.*, 64:2261, May 1990. DOI: [10.1103/PhysRevLett.64.2261](https://doi.org/10.1103/PhysRevLett.64.2261). URL <https://link.aps.org/doi/10.1103/PhysRevLett.64.2261>.
- [51] R. L. Walsworth, I. F. Silvera, E. M. Mattison, and R. F. C. Vessot. Test of the linearity of quantum mechanics in an atomic system with a hydrogen maser. *Phys. Rev. Lett.*, 64:2599, 1990. DOI: [10.1103/PhysRevLett.64.2599](https://doi.org/10.1103/PhysRevLett.64.2599). URL <https://link.aps.org/doi/10.1103/PhysRevLett.64.2599>.
- [52] P. K. Majumder, B. J. Venema, S. K. Lamoreaux, B. R. Heckel, and E. N. Fortson. Test of the linearity of quantum mechanics in optically pumped ${}^{201}\text{Hg}$. *Phys. Rev. Lett.*, 65:2931, 1990. DOI: [10.1103/PhysRevLett.65.2931](https://doi.org/10.1103/PhysRevLett.65.2931). URL <https://link.aps.org/doi/10.1103/PhysRevLett.65.2931>.
- [53] S. Forstner, M. Zych, S. Basiri-Esfahani, K. E. Khosla, and W. P. Bowen. Nanomechanical test of quantum linearity. *Optica*, 7:1427, 2020. DOI: [10.1364/OP-TICA.391671](https://doi.org/10.1364/OP-TICA.391671).
- [54] I. J. Arnquist, F. T. Avignone, A. S. Barabash, C. J. Barton, K. H. Bhimani, E. Blalock, B. Bos, M. Busch, M. Buuck, T. S. Caldwell, Y-D. Chan, C. D. Christof-

- erson, P.-H. Chu, M. L. Clark, C. Cuesta, J. A. Detwiler, Yu. Efremenko, H. Ejiri, S. R. Elliott, G. K. Giovanetti, M. P. Green, J. Gruszko, I. S. Guinn, V. E. Guisepppe, C. R. Haufe, R. Henning, D. Hervas Aguilar, E. W. Hoppe, A. Hostiuc, I. Kim, R. T. Kouzes, T. E. Lannen V., A. Li, A. M. Lopez, J. M. López-Castaño, E. L. Martin, R. D. Martin, R. Massarczyk, S. J. Meijer, T. K. Oli, G. Othman, L. S. Paudel, W. Pettus, A. W. P. Poon, D. C. Radford, A. L. Reine, K. Rielage, N. W. Ruof, D. Tedeschi, R. L. Varner, S. Vasilyev, J. F. Wilkerson, C. Wiseman, W. Xu, C.-H. Yu, and B. X. Zhu. Search for spontaneous radiation from wave function collapse in the Majorana Demonstrator. *Phys. Rev. Lett.*, 129:080401, 2022. DOI: [10.1103/PhysRevLett.129.080401](https://doi.org/10.1103/PhysRevLett.129.080401).
- [55] M. Polkovnikov, A. V. Gramolin, D. E. Kaplan, S. Rajendran, and A. O. Sushkov. Experimental limit on nonlinear state-dependent terms in quantum theory. *Phys. Rev. Lett.*, 130:040202, 2023. DOI: [10.1103/PhysRevLett.130.040202](https://doi.org/10.1103/PhysRevLett.130.040202).
- [56] J. Broz, B. You, S. Khan, H. Häffner, D. E. Kaplan, and S. Rajendran. Test of causal nonlinear quantum mechanics by Ramsey interferometry with a trapped ion. *Phys. Rev. Lett.*, 130:200201, 2023. DOI: [10.1103/PhysRevLett.130.200201](https://doi.org/10.1103/PhysRevLett.130.200201).
- [57] C. H. Bennett, E. Bernstein, G. Brassard, and U. Vazirani. Strengths and weaknesses of quantum computing. *SIAM J. Comput.*, 26:1510, 1997. DOI: [10.1137/S0097539796300933](https://doi.org/10.1137/S0097539796300933).
- [58] E. P. Gross. Structure of a quantized vortex in boson systems. *Nuovo Cimento*, 20:454, 1961. DOI: [10.1007/BF02731494](https://doi.org/10.1007/BF02731494).
- [59] L. P. Pitaevskii. Vortex lines in an imperfect Bose gas. *Sov. Phys. JETP*, 13:451, 1961.
- [60] L. Erdős and B. Schlein. Quantum dynamics with mean field interactions: A new approach. *J. Stat. Phys.*, 134:859, 2009. DOI: [10.1007/s10955-008-9570-7](https://doi.org/10.1007/s10955-008-9570-7).
- [61] M. R. Geller. The universe as a nonlinear quantum simulation: Large n limit of the central spin model. *Phys. Rev. A*, 108:042210, 2023. DOI: [10.1103/PhysRevA.108.042210](https://doi.org/10.1103/PhysRevA.108.042210). arXiv: 2112.09005.
- [62] E. H. Lieb and D. W. Robinson. The finite group velocity of quantum spin systems. *Comm. Math. Phys.*, 28:251, 1972. DOI: [10.1007/BF01645779](https://doi.org/10.1007/BF01645779).
- [63] Z. Idziaszek, T. Calarco, and P. Zoller. Controlled collisions of a single atom and an ion guided by movable trapping potentials. *Phys. Rev. A*, 76:033409, 2007. DOI: [10.1103/PhysRevA.76.033409](https://doi.org/10.1103/PhysRevA.76.033409).
- [64] M. Tomza, K. Jachymski, R. Gerritsma, A. Negretti, T. Calarco, Z. Idziaszek, and P. S. Julienne. Cold hybrid ion-atom systems. *Rev. Mod. Phys.*, 91:035001, 2019. DOI: [10.1103/RevModPhys.91.035001](https://doi.org/10.1103/RevModPhys.91.035001).
- [65] S. Jyothi, K. N. Egodapitiya, B. Bondurant, Z. Jia, E. Pretzsch, P. Chiappina, G. Shu, and K. R. Brown. A hybrid ion-atom trap with integrated high resolution mass spectrometer. *Rev. Sci. Instrum.*, 90:103201, 2019. DOI: [10.1063/1.5121431](https://doi.org/10.1063/1.5121431).
- [66] L. Karpa. Interactions of ions and ultracold neutral atom ensembles in composite optical dipole traps: Developments and perspectives. *Atoms*, 9:39, 2021. DOI: [10.3390/atoms9030039](https://doi.org/10.3390/atoms9030039).
- [67] R. S. Lous and R. Gerritsma. Ultracold ion-atom experiments: cooling, chemistry, and quantum effects. *Advances in Atomic, Molecular, and Optical Physics*, 71:65, 2022. DOI: [10.1016/bs.aamop.2022.05.002](https://doi.org/10.1016/bs.aamop.2022.05.002).
- [68] C. Zipkes, S. Palzer, C. Sias, and M. Kohl. A trapped single ion inside a Bose–Einstein condensate. *Nature*, 464:388, 2010. DOI: [10.1038/nature08865](https://doi.org/10.1038/nature08865).
- [69] J. Schmidt, P. Weckesser, F. Thielemann, T. Schaetz, and L. Karpa. Optical traps for sympathetic cooling of ions with ultracold neutral atoms. *Phys. Rev. Lett.*, 124:053402, 2020. DOI: [10.1103/PhysRevLett.124.053402](https://doi.org/10.1103/PhysRevLett.124.053402).

- [70] R. Gerritsma, A. Negretti, H. Doerk, Z. Idziaszek, T. Calarco, and F. Schmidt-Kaler. Bosonic Josephson junction controlled by a single trapped ion. *Phys. Rev. Lett.*, 109:080402, 2012. DOI: [10.1103/PhysRevLett.109.080402](https://doi.org/10.1103/PhysRevLett.109.080402).
- [71] J. Joger, A. Negretti, and R. Gerritsma. Quantum dynamics of an atomic double-well system interacting with a trapped ion. *Phys. Rev. A*, 89:063621, 2014. DOI: [10.1103/PhysRevA.89.063621](https://doi.org/10.1103/PhysRevA.89.063621).
- [72] M. R. Ebgha, S. Saeidian, P. Schmelcher, and A. Negretti. Compound atom-ion Josephson junction: Effects of finite temperature and ion motion. *Phys. Rev. A*, 100:033616, 2019. DOI: [10.1103/PhysRevA.100.033616](https://doi.org/10.1103/PhysRevA.100.033616).
- [73] C. E. Wieman, D. E. Pritchard, and D. J. Wineland. Atom cooling, trapping, and quantum manipulation. *Rev. Mod. Phys.*, 71:S253, 1999. DOI: [10.1103/RevModPhys.71.S253](https://doi.org/10.1103/RevModPhys.71.S253).
- [74] F. Dalfovo, S. Giorgini, L. P. Pitaevskii, and S. Stringari. Theory of Bose-Einstein condensation in trapped gases. *Rev. Mod. Phys.*, 71:463, 1999. DOI: [10.1103/RevModPhys.71.463](https://doi.org/10.1103/RevModPhys.71.463).
- [75] A. J. Leggett. Bose-Einstein condensation in the alkali gases: Some fundamental concepts. *Rev. Mod. Phys.*, 73:307, 2001. DOI: [10.1103/RevModPhys.73.307](https://doi.org/10.1103/RevModPhys.73.307).
- [76] O. Morsch and M. Oberthaler. Dynamics of Bose-Einstein condensates in optical lattices. *Rev. Mod. Phys.*, 78:179, 2006. DOI: [10.1103/RevModPhys.78.179](https://doi.org/10.1103/RevModPhys.78.179).
- [77] E. H. Lieb, R. Seiringer, and J. Yngvason. Bosons in a trap: A rigorous derivation of the Gross-Pitaevskii energy functional. *Phys. Rev. A*, 61:043602, 2000. DOI: [10.1103/PhysRevA.61.043602](https://doi.org/10.1103/PhysRevA.61.043602).
- [78] C. Bardos, F. Golse, and N. J. Mauser. Weak coupling limit of the N-particle Schrödinger equation. *Methods and Applications of Analysis*, 7:275, 2000.
- [79] C. Gokler. Mean field limit for many-particle interactions. arXiv: 2006.05486.
- [80] J. Fröhlich, S. Graffi, and S. Schwarz. Mean-field and classical limit of many-body Schrödinger dynamics for bosons. *Comm. Math. Phys.*, 271:681, 2007. DOI: [10.1007/s00220-007-0207-5](https://doi.org/10.1007/s00220-007-0207-5).
- [81] L. Erdős, B. Schlein, and H.-T. Yau. Rigorous derivation of the Gross-Pitaevskii equation. *Phys. Rev. Lett.*, 98:040404, 2007. DOI: [10.1103/PhysRevLett.98.040404](https://doi.org/10.1103/PhysRevLett.98.040404).
- [82] I. Rodnianski and B. Schlein. Quantum fluctuations and rate of convergence towards mean field dynamics. *Comm. Math. Phys.*, 291:31, 2009. DOI: [10.1007/s00220-009-0867-4](https://doi.org/10.1007/s00220-009-0867-4).
- [83] A. Knowles and P. Pickl. Mean-field dynamics: Singular potentials and rate of convergence. *Commun. Math. Phys.*, 298:101, 2010. DOI: [10.1007/s00220-010-1010-2](https://doi.org/10.1007/s00220-010-1010-2).
- [84] L. Chen, J. O. Lee, and B. Schlein. Rate of convergence towards Hartree dynamics. *J. Stat. Phys.*, 144:872, 2011. DOI: [10.1007/s10955-011-0283-y](https://doi.org/10.1007/s10955-011-0283-y).
- [85] Z. Ammari, M. Falconi, and B. Pawilowski. On the rate of convergence for the mean field approximation of many-body quantum dynamics. arXiv: 1411.6284v1.
- [86] P. Pickl. Derivation of the time dependent Gross-Pitaevskii equation with external fields. *Reviews in Mathematical Physics*, 27:1550003, 2015. DOI: [10.1142/S0129055X15500038](https://doi.org/10.1142/S0129055X15500038).
- [87] N. Benedikter, M. Porta, and B. Schlein. *Effective Evolution Equations from Quantum Dynamics*. Springer, Berlin, 2016. DOI: [10.1007/978-3-319-24898-1](https://doi.org/10.1007/978-3-319-24898-1).
- [88] J. Fröhlich, A. Knowles, B. Schlein, and V. Sohinger. A microscopic derivation of time-dependent correlation functions of the 1D cubic nonlinear Schrödinger equation. *Advances in Mathematics*, 353:67, 2019. DOI: [10.1016/j.aim.2019.06.029](https://doi.org/10.1016/j.aim.2019.06.029).
- [89] C. Brennecke and B. Schlein. Gross-Pitaevskii dynamics for Bose-Einstein condensates. *Analysis and PDE*, 12:1513, 2019. DOI: [10.2140/apde.2019.12.1513](https://doi.org/10.2140/apde.2019.12.1513).

- [90] A. Meill and D. A. Meyer. Mean field approximation for identical bosons on the complete graph. arXiv: 1910.14521.
- [91] V. Coffman, J. Kundu, and W. K. Wootters. Distributed entanglement. *Phys. Rev. A*, 61:052306, 2000. DOI: [10.1103/PhysRevA.61.052306](https://doi.org/10.1103/PhysRevA.61.052306).
- [92] T. J. Osborne and F. Verstraete. General monogamy inequality for bipartite qubit entanglement. *Phys. Rev. Lett.*, 96:220503, 2006. DOI: [10.1103/PhysRevLett.96.220503](https://doi.org/10.1103/PhysRevLett.96.220503).
- [93] D. Yang. A simple proof of monogamy of entanglement. *Phys. Lett. A*, 360:249, 2006. DOI: [10.1016/j.physleta.2006.08.027](https://doi.org/10.1016/j.physleta.2006.08.027).
- [94] X. Wang and K. Mølmer. Pairwise entanglement in symmetric multiqubit systems. *Eur. Phys. J. D*, 18:385, 2002. DOI: [10.1140/epjd/e20020045](https://doi.org/10.1140/epjd/e20020045).
- [95] B. Mielnik. Mobility of nonlinear systems. *J. Math. Phys.*, 21:44, 1980. DOI: [10.1063/1.524331](https://doi.org/10.1063/1.524331).
- [96] V. Gorini, A. Kossakowski, and E. C. G. Sudarshan. Completely positive dynamical semigroups of N -level systems. *J. Math. Phys.*, 17:821, 1976. DOI: [10.1063/1.522979](https://doi.org/10.1063/1.522979).
- [97] G. Lindblad. On the generators of quantum dynamical semigroups. *Comm. Math. Phys.*, 48:119, 1976.
- [98] M. M. Wilde. *Quantum Information Theory*. Cambridge University Press, 2017.
- [99] M. B. Ruskai. Beyond strong subadditivity? Improved bounds on the contraction of generalized relative entropy. *Rev. Math. Phys.*, 6:1147, 1994. DOI: [10.1142/S0129055X94000407](https://doi.org/10.1142/S0129055X94000407).
- [100] C. Ryu, E. C. Samson, and M. G. Boshier. Quantum interference of currents in an atomtronic SQUID. *Nat Commun.*, 11:3338, 2020. DOI: <https://doi.org/10.1038/s41467-020-17185-6>.
- [101] K. T. Kapale and J. P. Dowling. Vortex phase qubit: Generating arbitrary, counterrotating, coherent superpositions in Bose-Einstein condensates via optical angular momentum beams. *Phys. Rev. Lett.*, 95:173601, 2005. DOI: [10.1103/PhysRevLett.95.173601](https://doi.org/10.1103/PhysRevLett.95.173601).
- [102] C. Ryu, M. F. Andersen, P. Cladé, V. Natarajan, K. Helmerson, and W. D. Phillips. Observation of persistent flow of a Bose-Einstein condensate in a toroidal trap. *Phys. Rev. Lett.*, 99:260401, 2007. DOI: [10.1103/PhysRevLett.99.260401](https://doi.org/10.1103/PhysRevLett.99.260401).
- [103] A. Ramanathan, K. C. Wright, S. R. Muniz, M. Zelan, W. T. Hill III, C. J. Lobb, K. Helmerson, W. D. Phillips, and K. C. Campbell. Superflow in a toroidal Bose-Einstein condensate: An atom circuit with a tunable weak link. *Phys. Rev. Lett.*, 106:130401, 2011. DOI: [10.1103/PhysRevLett.106.130401](https://doi.org/10.1103/PhysRevLett.106.130401).
- [104] S. Eckel, J. G. Lee, F. Jendrzejewski, N. Murray, C. W. Clark, C. J. Lobb, W. D. Phillips, M. Edwards, and G. K. Campbell. Hysteresis in a quantized superfluid atomtronic circuit. *Nature*, 506:200, 2014. DOI: doi.org/10.1038/nature12958.
- [105] H. Kim, G. Zhu, J. V. Porto, and M. Hafezi. Optical lattice with torus topology. *Phys. Rev. Lett.*, 121:133002, 2018. DOI: [10.1103/PhysRevLett.121.133002](https://doi.org/10.1103/PhysRevLett.121.133002).
- [106] L. Pezzè, K. Khani, C. Daix, N. Grani, B. Donelli, F. Scazza, D. Hernandez-Rajkov, W. J. Kwon, G. Del Pace, and G. Roati. Stabilizing persistent currents in an atomtronic Josephson junction necklace. arXiv: 2311.05523.
- [107] F. D. M. Haldane. Geometrical interpretation of momentum and crystal momentum of classical and quantum ferromagnetic Heisenberg chains. *Phys. Rev. Lett.*, 57:1488, 1988. DOI: [10.1103/PhysRevLett.57.1488](https://doi.org/10.1103/PhysRevLett.57.1488).
- [108] K. Kraus. General state changes in quantum theory. *Ann. Phys.*, 64:311, 1971. DOI: [https://doi.org/10.1016/0003-4916\(71\)90108-4](https://doi.org/10.1016/0003-4916(71)90108-4).
- [109] M.-D. Choi. Completely positive linear maps on complex matrices. *Lin. Alg. App.*, 10:285, 1975.

- [110] P. Pechukas. Reduced dynamics need not be completely positive. *Phys. Rev. Lett.*, 73:1060, 1994. DOI: [10.1103/PhysRevLett.73.1060](https://doi.org/10.1103/PhysRevLett.73.1060).
- [111] A. Shaji and E. C. G. Sudarshan. Who's afraid of not completely positive maps? *Phys. Lett. A*, 341:48, 2005.
- [112] H. A. Carteret, D. R. Terno, and K. Życzkowski. Dynamics beyond completely positive maps: Some properties and applications. *Phys. Rev. A*, 77:042113, 2008. DOI: [10.1103/PhysRevA.77.042113](https://doi.org/10.1103/PhysRevA.77.042113).
- [113] J. M. Dominy, A. Shabani, and D. A. Lidar. A general framework for complete positivity. *Quantum Inf. Process.*, 15:465, 2016. DOI: [10.1007/s11128-015-1148-0](https://doi.org/10.1007/s11128-015-1148-0).
- [114] J. M. Dominy and D. A. Lidar. Beyond complete positivity. *Quantum Inf. Process.*, 15:1349, 2016. DOI: [10.1007/s11128-015-1228-1](https://doi.org/10.1007/s11128-015-1228-1).
- [115] E. C. G. Sudarshan, P. M. Mathews, and J. Rau. Stochastic dynamics of quantum-mechanical systems. *Phys. Rev.*, 121:920, 1961. DOI: <https://doi.org/10.1103/PhysRev.121.920>.
- [116] S. Krinner, N. Lacroix, A. Remm, A. Di Paolo, E. Genois, C. Leroux, C. Hellings, S. Lazar, F. Swiadek, J. Herrmann, G. J. Norris, C. K. Andersen, M. Müller, A. Blais, C. Eichler, and A. Wallraff. Realizing repeated quantum error correction in a distance-three surface code. *Nature*, 605:669, 2022. DOI: [10.1038/s41586-022-04566-8](https://doi.org/10.1038/s41586-022-04566-8).
- [117] R. Acharya, I. Aleiner, R. Allen, T. I. Andersen, M. Ansmann, F. Arute, K. Arya, A. Asfaw, J. Atalaya, and R. Babbush *et al.* Suppressing quantum errors by scaling a surface code logical qubit. *Nature*, 614:676, 2023. DOI: [10.1038/s41586-022-05434-1](https://doi.org/10.1038/s41586-022-05434-1).
- [118] D. C. McKay, I. Hincks, E. J. Pritchett, M. Carroll, L. C. G. Govia, and S. T. Merkel. Benchmarking quantum processor performance at scale. arXiv: 2311.05933.
- [119] D. Bluvstein, H. Levine, G. Semeghini, T. T. Wang, S. Ebadi, M. Kalinowski, A. Keesling, N. Maskara, H. Pichler, M. Greiner, V. Vuletić, and M. D. Lukin. A quantum processor based on coherent transport of entangled atom arrays. *Nature*, 604:451, 2022. DOI: [10.1038/s41586-022-04592-6](https://doi.org/10.1038/s41586-022-04592-6).
- [120] T. M. Graham, Y. Song, J. Scott, C. Poole, L. Phuttitarn, K. Jooya, P. Eichler, X. Jiang, A. Marra, B. Grinkemeyer, M. Kwon, M. Ebert, J. Cherek, M. T. Lichtman, M. Gillette, J. Gilbert, D. Bowman, T. Ballance, C. Campbell, E. D. Dahl, O. Crawford, N. S. Blunt, B. Rogers, T. Noel, and M. Saffman. Multi-qubit entanglement and algorithms on a neutral-atom quantum computer. *Nature*, 604:457, 2022. DOI: [10.1038/s41586-022-04603-6](https://doi.org/10.1038/s41586-022-04603-6).
- [121] L. Egan, D. M. Debroy, C. Noel, A. Risinger, D. Zhu, D. Biswas, M. Newman, M. Li, K. R. Brown, M. Cetina, and C. Monroe. Fault-tolerant control of an error-corrected qubit. *Nature*, 598:281, 2022. DOI: [10.1038/s41586-021-03928-y](https://doi.org/10.1038/s41586-021-03928-y).
- [122] S. A. Moses, C. H. Baldwin, M. S. Allman, R. Ancona, L. Ascarrunz, C. Barnes, J. Bartolotta, B. Bjork, P. Blanchard, M. Bohn, J. G. Bohnet, N. C. Brown, N. Q. Burdick, W. C. Burton, S. L. Campbell, J. P. Campora, C. Carron, J. Chambers, J. W. Chan, Y. H. Chen, A. Chernoguzov, E. Chertkov, J. Colina, J. P. Curtis, R. Daniel, M. DeCross, D. Deen, C. Delaney, J. M. Dreiling, C. T. Ertsgaard, J. Esposito, B. Estey, M. Fabrikant, C. Figgatt, C. Foltz, M. Foss-Feig, D. Francois, J. P. Gaebler, T. M. Gatterman, C. N. Gilbreth, J. Giles, E. Glynn, A. Hall, A. M. Hankin, A. Hansen, D. Hayes, B. Higashi, I. M. Hoffman, B. Horning, J. J. Hout, R. Jacobs, J. Johansen, L. Jones, J. Karcz, T. Klein, P. Lauria, P. Lee, D. Liefer, S. T. Lu, D. Lucchetti, C. Lytle, A. Malm, M. Matheny, B. Mathewson, K. Mayer, D. B. Miller, M. Mills, B. Neyenhuis, L. Nugent, S. Olson, J. Parks, G. N. Price, Z. Price, M. Pugh, A. Ransford, A. P. Reed, C. Roman, M. Rowe, C. Ryan-Anderson, S. Sanders, J. Sedlacek, P. Shevchuk, P. Siegfried, T. Skripka, B. Spaun, R. T.

- Sprenkle, R. P. Stutz, M. Swallows, R. I. Tobey, A. Tran, T. Tran, E. Vogt, C. Volin, J. Walker, A. M. Zolot, and J. M. Pino. A race track trapped-ion quantum processor. *Phys. Rev. X*, 13:041052, 2023. DOI: [10.1103/PhysRevX.13.041052](https://doi.org/10.1103/PhysRevX.13.041052).
- [123] W. K. Woiters. Entanglement of formation of an arbitrary state of two qubits. *Phys. Rev. Lett.*, 80:2245–8, 1998. DOI: [10.1103/PhysRevLett.80.2245](https://doi.org/10.1103/PhysRevLett.80.2245).
- [124] R. Horodecki, P. Horodecki, M. Horodecki, and K. Horodecki. Quantum entanglement. *Rev. Mod. Phys.*, 81:865, 2009. DOI: [10.1103/RevModPhys.81.865](https://doi.org/10.1103/RevModPhys.81.865).
- [125] X.-L. Zong, H.-H. Yin, W. Song, and Z.-L. Cao. Monogamy of quantum entanglement. arXiv: 2201.00366.
- [126] M. A. Nielsen and I. L. Chuang. *Quantum Computation and Quantum Information*. Cambridge University Press, Cambridge, England, 2000.